2011

THE SYNTHESIS, CHARACTERIZATION, AND UPCONVERTING PROPERTIES OF ERBIUM DOPED; YTTERBIUM, ERBIUM CO-DOPED YTTRIUM OXYSULFIDE PHOSPHORS UNDER 808, 980, AND 1560 nm EXCITATION

James Wilkins
Virginia Commonwealth University

THE SYNTHESIS, CHARACTERIZATION, AND UPCONVERTING PROPERTIES OF ERBIUM DOPED; YTTERBIUM, ERBIUM CO-DOPED YTTRIUM OXYSULFIDE PHOSPHORS UNDER 808, 980, AND 1560 nm EXCITATION

A thesis submitted in partial fulfillment of the requirements for the degree, Master of Chemistry at Virginia Commonwealth University.

by

James Robert Wilkins
Bachelor of Science, Chemistry
Virginia Commonwealth University
May 2008

Director: Dr. Garry P. Glaspell,
Associate Research Professor, Department of Chemistry

Virginia Commonwealth University
Richmond, Virginia
May 2011

Acknowledgement

The author would like to thank a number of persons. First and foremost, I send thanks to my mother and father, for giving me the opportunity to experience life. Also, I would like to thank my brother for his support and also for being a cool guy. I would like to thank Dr. Garry Glaspell for informative discussions and technical guidance with this project. I would like to thank Dr. John Anderson for generously allowing me to have unlimited access to his lab and spectroscopy equipment which helped make this all possible.

Table of Contents

List of Figures

Figures Page

List of Abbreviations

Abbreviations Page

a.u. ..... Arbitrary Units

cps ..... Counts Per Second (Photons)

°C ..... Celsius (degrees)

Em. ..... Emission

ESA ..... Excited State Absorption

ET ..... Energy Transfer

GSA ..... Ground State Absorption

h ..... Hours

Int. ..... Intensity

IR ..... Infrared

kV ..... Kilovolt

kW ..... Kilowatt

μW ..... Microwatt

mA ..... Microamp

mW ..... Milliwatt

mol % ..... Mole Percent

NIR ..... Near Infrared

nm ..... Nanometer

QD ..... Quantum Dot Semiconductor

RE ..... Rare Earth

SEM ..... Scanning Electron Microscope

TEM ..... Transmission Electron Microscopy

UC ..... Upconversion or Upconverting

UV ..... Ultraviolet

VIS ..... Visible

Wt. % ..... Weight Percent

XRD ..... X – Ray Diffraction

Abstract

Bulk yttrium oxysulfide phosphors were prepared using the polysulfide flux method. The morphology and structure was characterized using transmission electron microscopy and x-ray powdered diffraction. Visible emissions occurring near 530 and 550 nm and 660 - 670 nm consistent with the $^2H_{11/2}$, $^4S_{3/2} \rightarrow {}^4I_{15/2}$ and $^4F_{9/2} \rightarrow {}^4I_{15/2}$ transitions, respectively, were observed under 808, 980, and 1560 nm excitation. The upconverting mechanisms excited at 808, 980, and 1560 nm have been investigated in detail. The power dependent behavior of the upconverted emission intensities for singly doped erbium phosphors excited at 808 and 980 nm indicated a two-photon excitation process. Likewise, the ytterbium and erbium co-doped phosphors excited at 980 nm also indicated a two-photon excitation process. Doping with 10% erbium showed the most intense emissions under 808 and 1560 nm excitation. Yttrium oxysulfide co-doped with 15% ytterbium and 3% erbium showed the most intense emissions under 980 nm excitation. Upon 1560 nm excitation, the intensity of the red emission band was significantly enhanced by co-doping erbium with ytterbium. Concentration quenching became apparent when either the concentration of erbium or ytterbium reached 20%.

1. Introduction

High energy ultraviolet (UV) radiation is typically used as the excitation source for the majority of visibly luminescent compounds. The emission produced (usually in the visible region of the electromagnetic spectrum) after the absorption of a single UV photon is a process known as fluorescence. Well known fluorescent compounds such as organic dyes, quantum dot semiconductors (QDs), and downconverters have been well studied for use in a variety of applications. However, for applications involving remote sensing, it is disadvantageous to use UV excited fluorescent compounds mainly due to autofluorescence of background objects caused by the excitation source. Organic dyes are not only susceptible to photobleaching (degradation of photostability) but also require certain pH conditions in order to maintain stability and function properly. More robust than organic dyes, QDs are considered unsafe for practical use in biological and environmental applications due to the elements from which they are made from cadium (Cd^{2+}), lead (Pb^{2+}), and selenium (Se^{2+}). The doping of rare earths (RE) more specifically europium (Eu^{3+}) and terbium (Tb^{3+}) into host crystalline structures where VIS emissions caused by the absorption of a single UV photon is referred to as downconversion. Downconverters have much better spectral characteristics than organic dyes and QDs which include narrow line emission bands, large Stokes' shifts, and longer excited state lifetimes.[1], [2] Nonetheless, highly selective optical reporters using organic dyes, quantum dot semiconductors, and downconverters have been demonstrated successfully leading to the development of new materials and ideas. The use of upconverting phosphors as optical probes is advantageous for remote sensing applications since the

excitation source is in the IR region eliminating the possibility of autofluorescence and need for time-resolved detection.

Upconversion (UC) differs from downconversion in that it is a process that converts multiple near-infrared (NIR) low energy photons into a higher energy UV or VIS photon by either step-wise excited state absorption (ESA) or energy transfer (ET) processes. ESA, typically a two-photon UC process usually only occurs at low level doping concentrations of a single RE ion type. It is a single ion mechanism where a photon from the incident source of radiation excites the ion from its ground state to an intermediate excited state. Excitation from the ground state to an intermediate excited state is known as ground state absorption (GSA). The absorption of the second photon then excites the ion to a higher excited state. Similar to ESA, the ET UC process occurs at higher level doping concentrations. In the ET process, photons from the incident source of radiation excite two separate localized ions in close proximity to an intermediate excited state. From here one ion will act as a sensitizer, relax, and non-radiatively transfer its energy to the neighboring ion resulting in the population of a higher emitting state. Radiative transitions back to the ground state result in visible emissions.[3] The nature of these processes is dependent upon the RE dopant types and concentrations within an optically inactive host lattice. Many host lattices have been used for UC which include but not limited to oxides, oxysulfides, and halides.[4-11] The REs' *4f* electrons are well shielded by the outer *5s* and *5p* orbitals therefore little interaction exists

between the host lattice and the RE *4f* electrons. This allows for the REs' excited states to remain at particular energies which result in strong narrow-line emissions.[12]

Erbium (Er^{3+}) has been the most extensively studied activator ion for UC due to its unique electronic energy level design of uniformly spaced long-lived excited states.[13] This allows Er^{3+} to exhibit UC luminescence at multiple different NIR excitation wavelengths including 808, 980, and 1560 nm. However, most literature articles on UC report using a 980 nm laser diode as there excitation source. Thus, many phosphors are sensitized with ytterbium (Yb^{3+}) in order to increase the conversion efficiency. Yb^{3+} has a high absorption cross-section in the NIR regime (~ 1000 nm) making it a first-rate sensitizer to 980 nm radiation. Co-doping Er^{3+} with Yb^{3+} increases the efficiency of the 980 nm UC process due to the spectral overlap of (Yb^{3+}) $^2F_{5/2} \rightarrow {}^2F_{7/2}$ NIR emission band and (Er^{3+}) $^4I_{11/2} \leftarrow {}^4I_{15/2}$ absorption band and the majority of visible light generated is due to the resonant ET from Yb^{3+} to Er^{3+}.[14]

Research in the upconverting technology field is currently being contributed to a variety of promising applications involving sensors, displays, backlights, anti-forgery markings, and communication optics.[15-17] The Yb^{3+}, Er^{3+} co-doped oxysulfide phosphors (Ln_2O_2S, Ln = Y^{3+}, Yttrium; La^{3+}, Lanthanum; or Gd^{3+}, Gadolinium) are currently the market's best green upconverting material with medium phonon energy (~ 520 cm^{-1}) under 980 nm excitation. It is well known that the halide lattices have the lowest phonon energies and are the most efficient UC materials known to date. However, they are not considered chemically stable or environmentally safe for practical use and also are

moisture sensitive. In comparison, the Y_2O_2S phosphor is not only environmentally friendly but also has much better stability both chemically and thermodynamically.[17] Thus, Y_2O_2S is a promising host material in various luminescent applications both current and future.

Various techniques have been reported for synthesizing RE doped UC oxysulfide phosphors including co- and homogenous precipitation, solution combustion, hydrothermal and solvothermal processes, and solid state flux methods.[2, 18-22] However, most of what is reported still requires multiple step processing, high temperatures, lengthy reaction times, and an inert, reducing or sulfurizing atmosphere in order to completely synthesize pure phase oxysulfide phosphors.

Currently, there are few articles available which report on the UC luminescence properties of bulk (micron-sized) $Y_2O_2S:Er^{3+}$, (Yb^{3+}, Er^{3+}) phosphors with respect to dopant concentrations under NIR excitation. Most of what is reported discuss the UC luminescence properties associated with nano-sized oxysulfide phosphors (particle sizes < 100 nm) under 980 nm NIR excitation only. Here, we take advantage of Er^{3+} unique electronic energy level design and report for the first time the UC luminescence properties and mechanisms related to $Y_2O_2S:Er^{3+}$, (Yb^{3+}, Er^{3+}) phosphors with varying doping concentrations under 808, 980, and 1560 nm radiation. To achieve this goal, the well known polysulfide flux method was used to synthesize the bulk $Y_2O_2S:Er^{3+}$, (Yb^{3+}, Er^{3+}) doped phosphors.[22-24] The as-prepared oxysulfide phosphors are produced in a single step and in high purity after washing with dilute acid.

2. Experimental

2.1 Reagents Used

Yttrium(III) oxide (99.99% Y_2O_3), Ytterbium(III) oxide (99.9% Yb_2O_3), Erbium(III) oxide (99.9% Er_2O_3), Sodium carbonate (ReagentPlus ≥ 99.0% Na_2CO_3), and Lithium carbonate (purum ≥ 99.0% Li_2CO_3) were purchased from Sigma Aldrich. Sulfur powder (~ 100 mesh, 99.5% S) was purchased from Alfa Aesar and Potassium phosphate tribasic heptahydrate (ACS grade ≥ 98.0%, $K_3PO_4 \cdot 7H_2O$) was purchased from VWR. All reagents were used without any further purification treatment.

2.2 Synthesis

The $Y_{(2-x-y)}O_2S:Yb_x^{3+}$, Er_y^{3+} upconverting phosphors were prepared in a single step using a modified solid state method involving a $Na_2CO_3/Li_2CO_3/K_3PO_4$-Sulfur flux in a reducing environment. In a typical experiment, stoichometric amounts of Y_2O_3, Yb_2O_3, and Er_2O_3 were thoroughly mixed in methanol. Once air dried the RE oxide mixture was ground with Na_2CO_3 (50 wt % of Y_2O_3), S (80 wt % of Y_2O_3), Li_2CO_3 (8 wt % of Y_2O_3), and K_3PO_4 $7H_2O$ (20 wt % of Y_2O_3) using an agate mortar and pestle. The precursor mixture was transferred to a small alumina crucible and covered. The covered crucible was then placed inside a larger crucible containing an excess of activated carbon. This was also covered in order to maintain the reducing atmosphere needed to inhibit the formation of oxides. The oxysulfide precursor mixture was then heat treated in a Thermo Scientific Type FD1545M Furnace for 3h at 1100°C at a ramp rate of 10°C min^{-1}. After

cooling to room temperature, the as-formed product was collected and washed with 5% (v/v) 70% HNO_3 and DI H_2O several times and dried overnight at 70°C in a vacuum oven.

2.3 Characterization Techniques

The morphology and structure of the as-prepared particles were characterized using TEM (Joel JEM-1230 operated at 120 kV) and XRD (X'Pert Philips Materials Research diffractometer, with Cu Kα radiation). The upconverting luminescence spectra were obtained using a Tau 3 steadystate and lifetime (Horiba Jobin Yvon) spectrofluormeter equipped with external, continuous wave 808, 980, and 1560 nm OEM lab lasers (Laserglow Technologies). It should be noted that the output power for each laser is adjustable therefore a Newport power meter Model 2930C was used to accurately determine the output power necessary for power dependence measurements.

3. Results and Discussion

3.1 Morphology and Structure

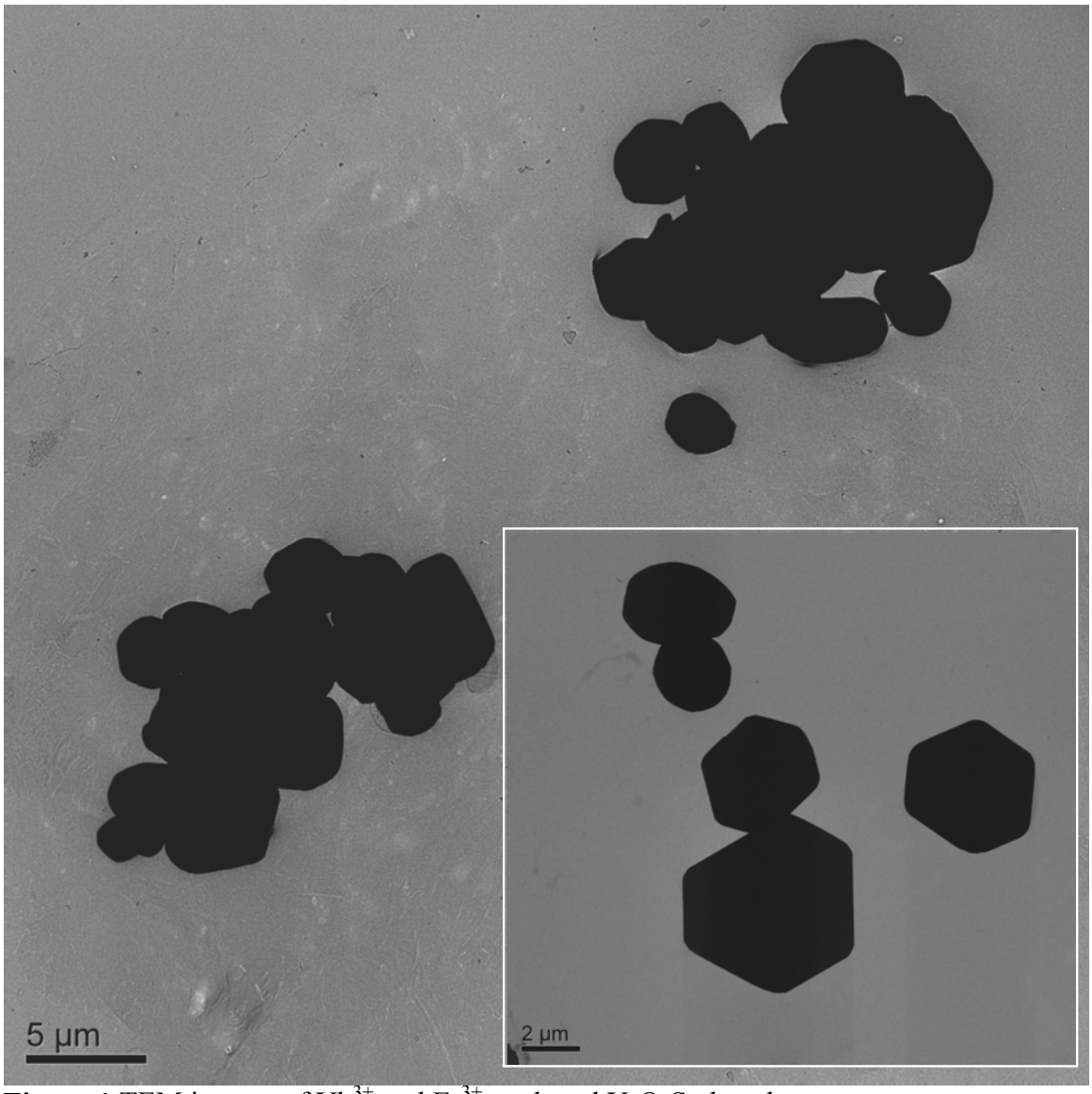

Figure 1 TEM images of Yb^{3+} and Er^{3+} co-doped Y_2O_2S phosphors.

Figure 1 displays a typical TEM image of an as-prepared oxysulfide sample doped with 5% (mol) Yb^{3+} and 1% Er^{3+}. The oxysulfide phosphors clearly exhibit a spherical morphology with the exception of a few irregular hexagonal facet pieces (shown in the inset). A wide particle size distribution ranging from 2 - 5 μm is clearly observed. However, using the Scherer equation the crystallite size was determined to be 35 nm, respectively. Thus, the irregular morphology and large distribution of particle sizes is attributed to the aggregation of crystallites which had agglomerated during the calcination process in order to minimize the surface area energy resulting in large particle formations. It should be noted that similar results have also been reported using a combustion synthesis for the preparation of oxysulfide phosphors. High and low-resolution SEM images demonstrated that the 10 - 30 μm particles were actually comprised of numerous much smaller particles ranging from 100 to 200 nm that had agglomerated to form large porous structures.[19]

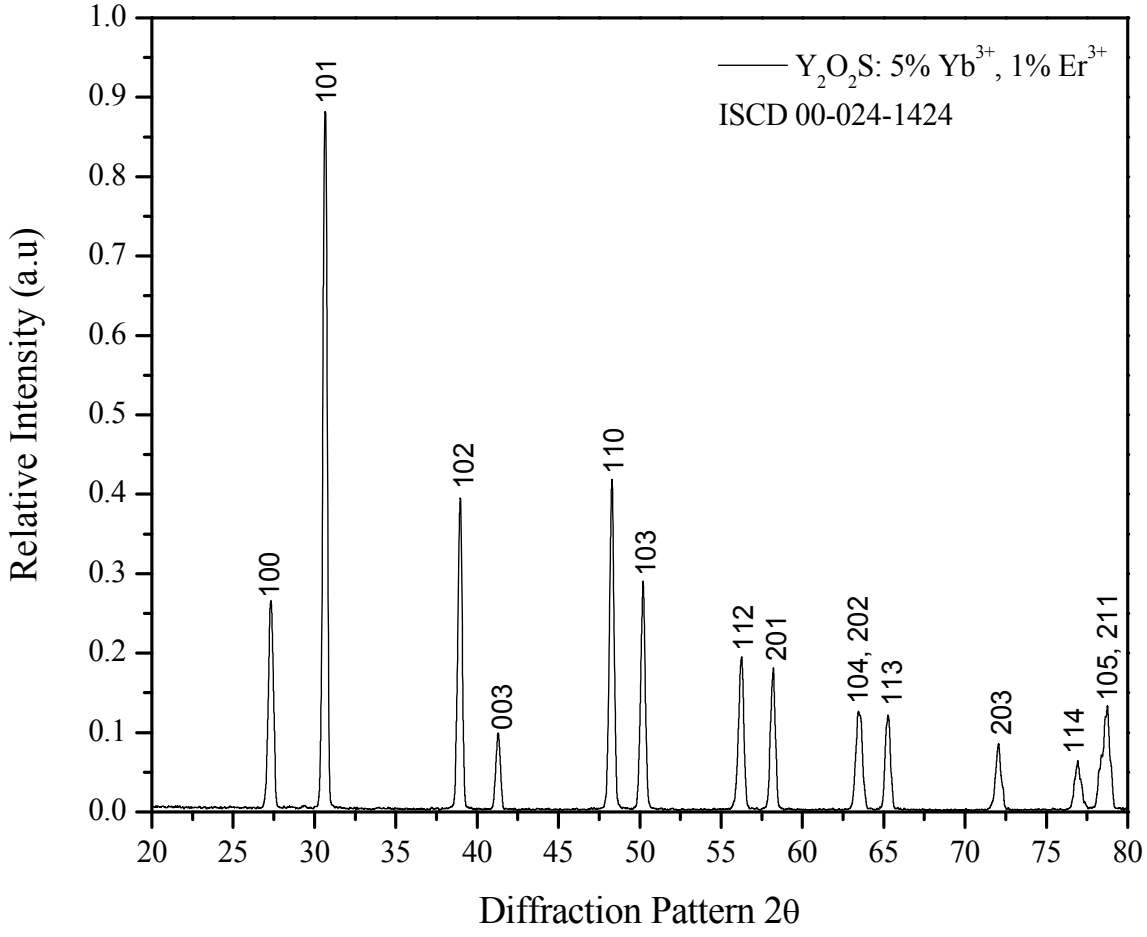

Figure 2 XRD pattern of an Y_2O_2S sample prepared using the polysulfide flux method showing pure hexagonal phase with the hkl crystalline planes shown.

Figure 2 shows the XRD powder diffraction pattern of the corresponding 5% Yb^{3+}, 1% Er^{3+} co-doped Y_2O_2S sample from Figure 1 matching the ICSD Index file 00-024-1424. It is important to note that only Y_2O_2S is observed with no sign of Y_2O_3 or fluxing agents present which is indicative that the sulfurization process of Y_2O_3 was complete. Also, the absence of Yb_2O_2S and Er_2O_2S diffraction peaks suggests that the Yb^{3+} and Er^{3+} ions are well dispersed throughout the Y_2O_2S lattice. Thus, Yb^{3+} and Er^{3+} co-doped Y_2O_2S phosphors can successfully be prepared at 1100°C for 3h in high purity using the methodology described here.

3.2 IR to VIS Upconversion

3.2.1 $Y_2O_2S:Er^{3+}$ Phosphors

3.2.1.1 808 nm Excitation

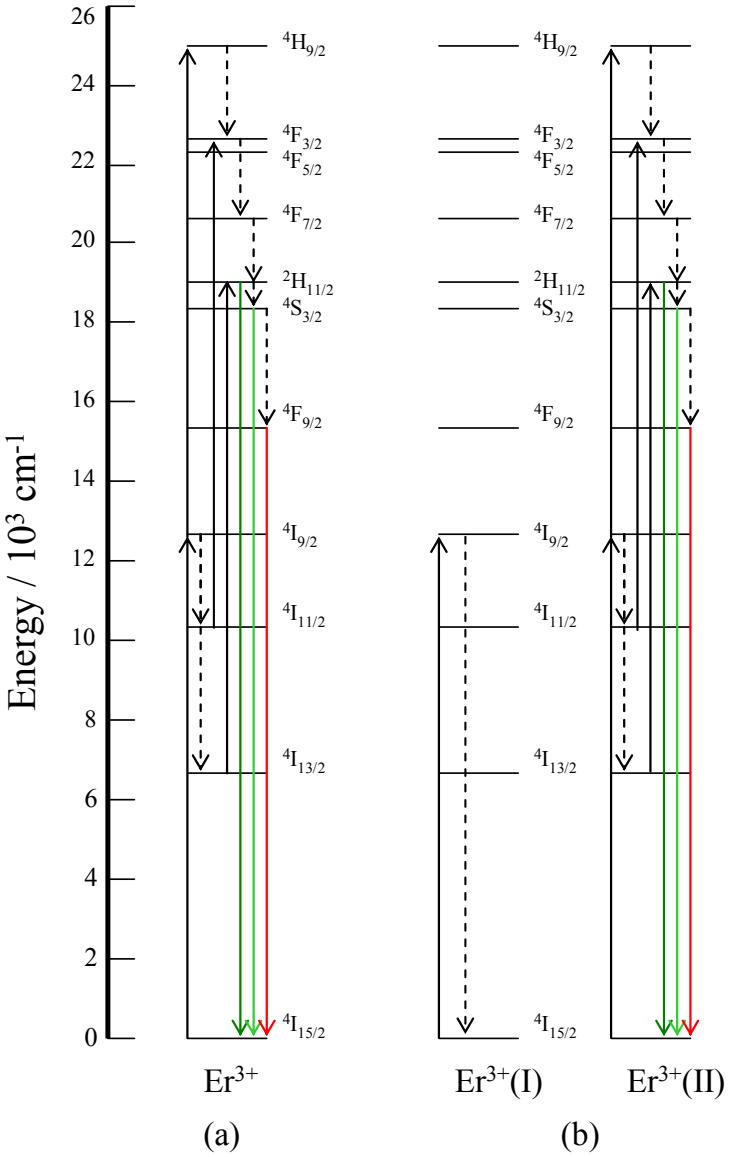

Figure 3 Schematic: (a) ESA and (b) ET UC processes occurring at the $^4I_{13/2}$, $^4I_{11/2}$, and $^4I_{9/2}$ states under 808 nm excitation.

The energy level schematic of the ESA and ET UC processes occurring at the $^4I_{13/2}$, $^4I_{11/2}$ and $^4I_{9/2}$ states along with the luminescence emissions and non-radiative transitions under 808 nm excitation are shown in Figure 3, a and b. In the ESA process (Figure 3a), a single Er^{3+} ion is excited from the $^4I_{15/2}$ ground state to the $^4I_{9/2}$ excited state, via GSA. A second 808 nm photon then excites Er^{3+} from the $^4I_{9/2}$ state to the higher $^2H_{9/2}$ state. ESA is also known to occur at the $^4I_{11/2}$ state as the result of non-radiative decay from the $^4I_{9/2}$ state after the absorption of the initial photon. A second incoming photon is then absorbed and excites Er^{3+} to the higher $^4F_{3/2}$ state. Alternatively, Er^{3+} ions that non-radiatively decay to the $^4I_{11/2}$ state can decay again to the $^4I_{13/2}$ state where ESA of a second photon results in the population of the $^2H_{11/2}$ emitting state. In the ET process (Figure 3b), two neighboring Er^{3+} ions are simultaneously excited to the $^4I_{9/2}$ state. From here, one Er^{3+} ion will relax back to the $^4I_{15/2}$ ground state and transfer its energy to the neighboring Er^{3+} ion resulting in the direct population of the higher $^2H_{9/2}$ state. Alternatively, one Er^{3+} ion can non-radiatively decay to either the $^4I_{11/2}$ or the $^4I_{13/2}$ states where ET from the neighboring Er^{3+} ion results in population of the $^4F_{3/2}$ and $^2H_{11/2}$ states.[25] A series of non-radiative transitions from the higher $^4H_{9/2}$ and $^4F_{3/2}$ states result in the population of the $^2H_{11/2}$, $^4S_{3/2}$ and $^4F_{9/2}$ emitting states where spin-allowed transitions back to the $^4I_{15/2}$ ground state result in green emissions around 530 and 550 nm and red emissions around 660 - 670 nm.

It is important to mention that the room temperature UC emission spectra obtained for all samples, independent of dopant concentration and excitation wavelength

have the same spectral profile where the green and red emissions occurring near 530 and 550 nm and 660 - 670 nm are consistent with the $(^2H_{11/2})^4S_{3/2} \rightarrow {}^4I_{15/2}$ and $^4F_{9/2} \rightarrow {}^4I_{15/2}$ transitions, respectively.

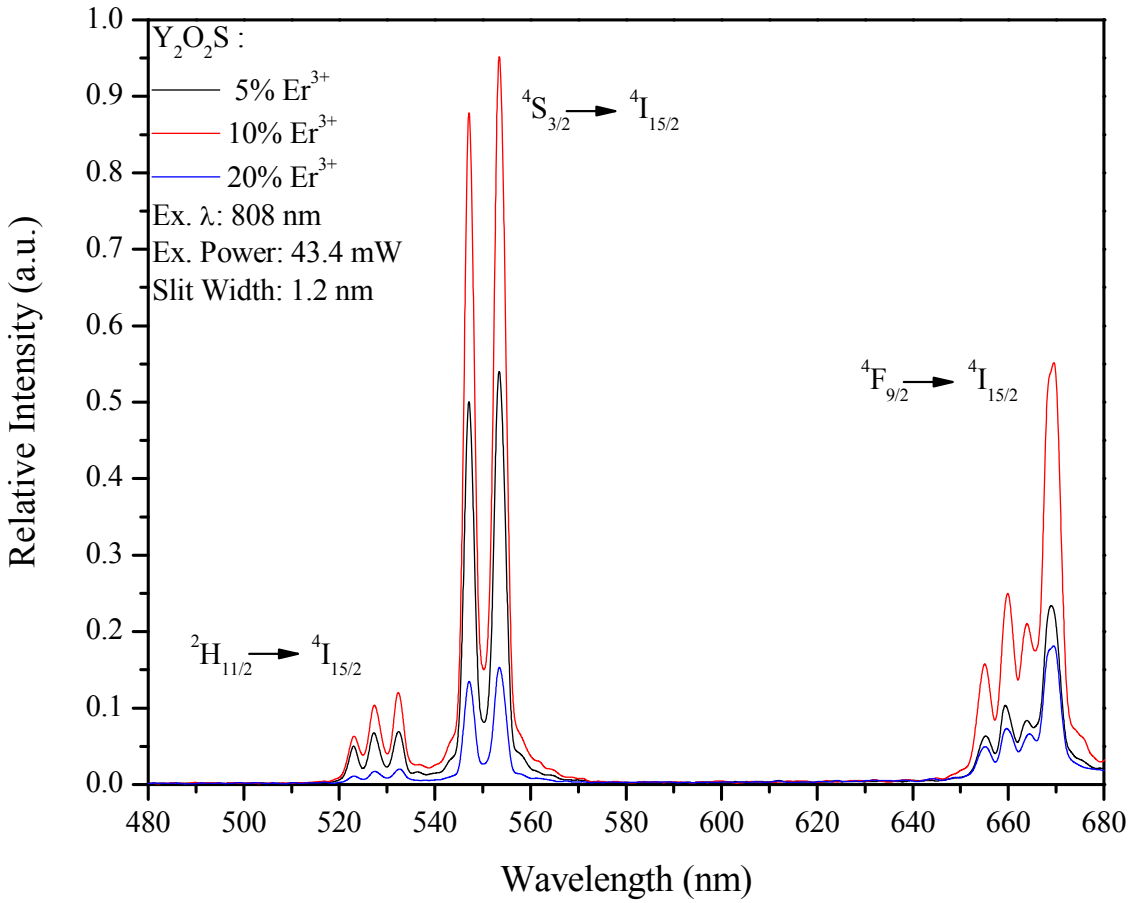

Figure 4 UC emission spectra of Y_2O_2S phosphors doped with 5%, 10% and 20% Er^{3+}.

Figure 4 shows the room temperature UC emission spectra of Y_2O_2S phosphors doped with 5%, 10%, and 20% Er^{3+} under 808 nm excitation operating with an output power of 43.4 mW. Doubling the Er^{3+} concentration from 5% to 10% showed significant enhancement on the luminescence intensity for both the green and red emission bands.

This increase in emission intensity is a result of ET between Er^{3+} ions in close proximity. When compared to the 5% Er^{3+} doped sample, the intensity of the green emission for the 20% Er^{3+} doped sample decreased considerably as result of concentration quenching where Er^{3+} ions are no longer able to reach the $^2H_{11/2}$ emitting state. However, the intensity of the red emission for both the 5 and 20% Er^{3+} doped samples remained about the same, respectively. This is because there are two different pathways in which the $^4F_{9/2}$ state can most likely be populated when excited by 808 nm: (1) relaxation from the $^2H_{11/2}$ state and (2) the $^4I_{9/2}$ Er^{3+}(I) + $^4I_{11/2}$ Er^{3+}(II) → $^4F_{13/2}$ Er^{3+}(I) + $^4F_{9/2}$ Er^{3+}(II) cross-relaxation process.[7], [25] This alternate pathway for populating the $^4F_{9/2}$ emitting state shown below in Figure 5 could possibly be responsible for the majority of red luminescence being emitted in high Er^{3+} doped oxysulfide phosphors under 808 nm excitation.

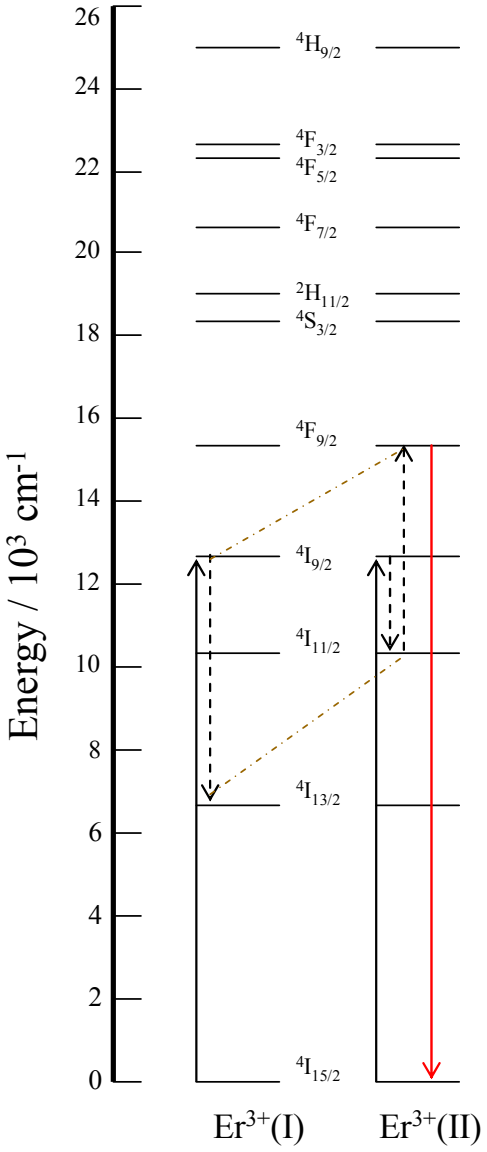

Figure 5 Schematic: $^4I_{9/2}Er^{3+}(I) + {}^4I_{11/2}Er^{3+}(II) \rightarrow {}^4F_{13/2}Er^{3+}(I) + {}^4F_{9/2}Er^{3+}(II)$ cross-relaxation process possibly responsible for the $^4F_{9/2}$ state in high Er^{3+} doped oxysulfide phosphors under 808 nm excitation.

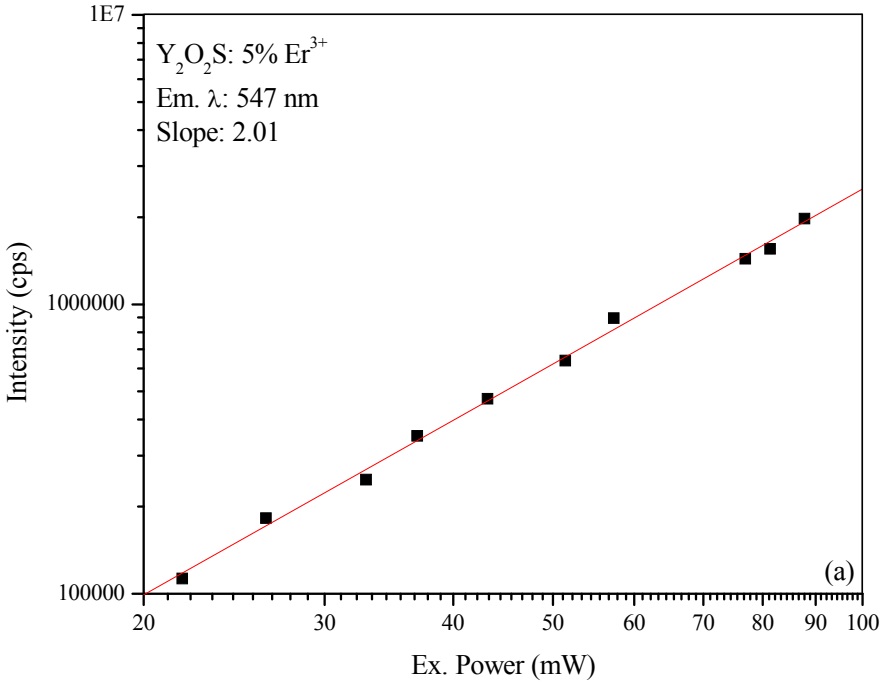
1E7
1000000
100000
Intensity (cps)
Y_2O_2S: 5% Er^{3+}
Em. λ: 547 nm
Slope: 2.01
(a)
20
30
40
50
60
70
80
90
100
Ex. Power (mW)

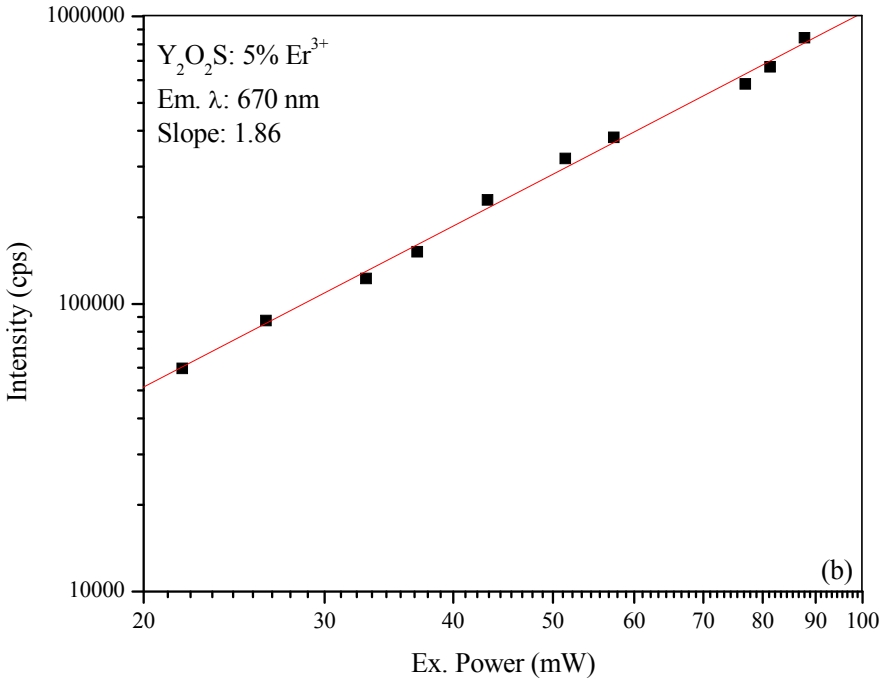
1000000
100000
10000
Intensity (cps)
Y_2O_2S: 5% Er^{3+}
Em. λ: 670 nm
Slope: 1.86
(b)
20
30
40
50
60
70
80
90
100
Ex. Power (mW)

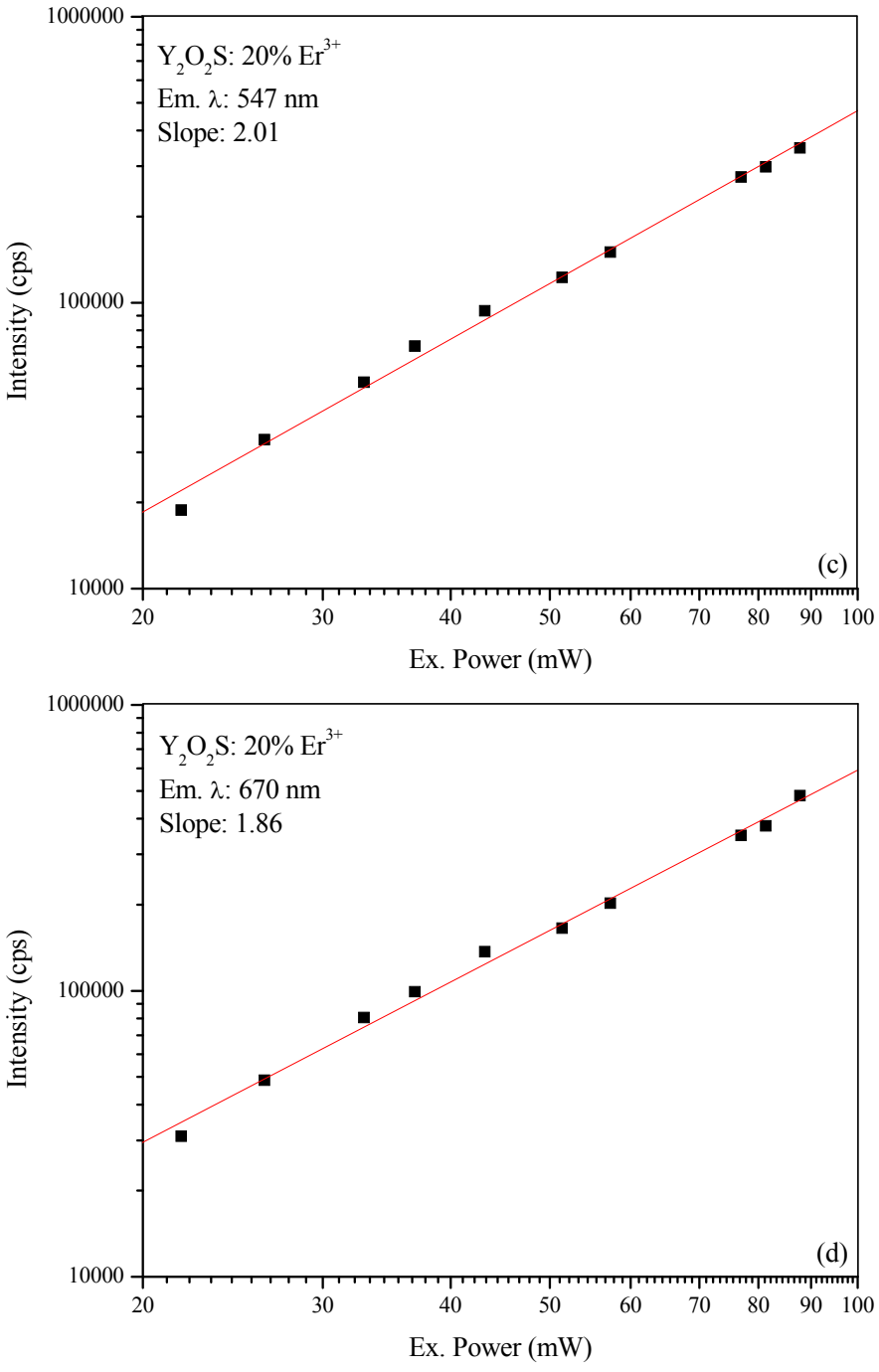

Figure 6 Power dependence of UC intensity of Y_2O_2S phosphors doped with 5% Er^{3+} and 20% Er^{3+} monitored at (a), (c) 547 nm, and (b), (d) 670 nm under 808 nm excitation.

It is well known that the UC intensity (I) and the excitation power (P) are dependant upon one another according to the equation $I \approx P^n$, where n is the number of NIR photons required to excite ions to a higher emitting state. The slope from a $\log_{10}$ scale where the luminescent emission intensity of a particular wavelength plotted against the excitation power will give the number of NIR pumping photons used in the UC process. It should be noted, that all power dependence measurements were made monitoring the 547 and 670 nm emission peaks which were the most intense in the green and red spectral regions.

Figure 6 shows the power dependence of UC intensity of Y_2O_2S phosphors doped with (a), (b) 5% Er^{3+}, and (c), (d) 20% Er^{3+}. From the power dependence plots, the UC emissions monitored at 547 nm and 670 nm required 2.01 and 1.86 photons for both the 5% Er^{3+} and 20% Er^{3+} doped samples. Even though the number of NIR pumping photons required to populate the $^4S_{3/2}$ and $^4F_{9/2}$ emitting states for both the 5% and 20% Er^{3+} doped sample remained the same, respectively, it does not necessarily rule out the possibility of this cross-relaxation mechanism. Population of the $^4F_{9/2}$ emitting state either by, the non-radiative $^2H_{11/2} \rightarrow {}^4F_{9/2}$ transition or the $^4I_{9/2}\ Er^{3+}(I) + {}^4I_{11/2}\ Er^{3+}(II) \rightarrow {}^4F_{13/2}\ Er^{3+}(I) + {}^4F_{9/2}\ Er^{3+}(II)$ cross-relaxation mechanism would still require a two-photon excitation process. However, it is most likely that the decrease in intensity observed in both the green and red emission bands is due to concentration quenching where the back transfer of energy between the Er^{3+} ions results in inefficient UC and at a 20% doping concentration this would be expected.

3.2.1.2 980 nm Excitation

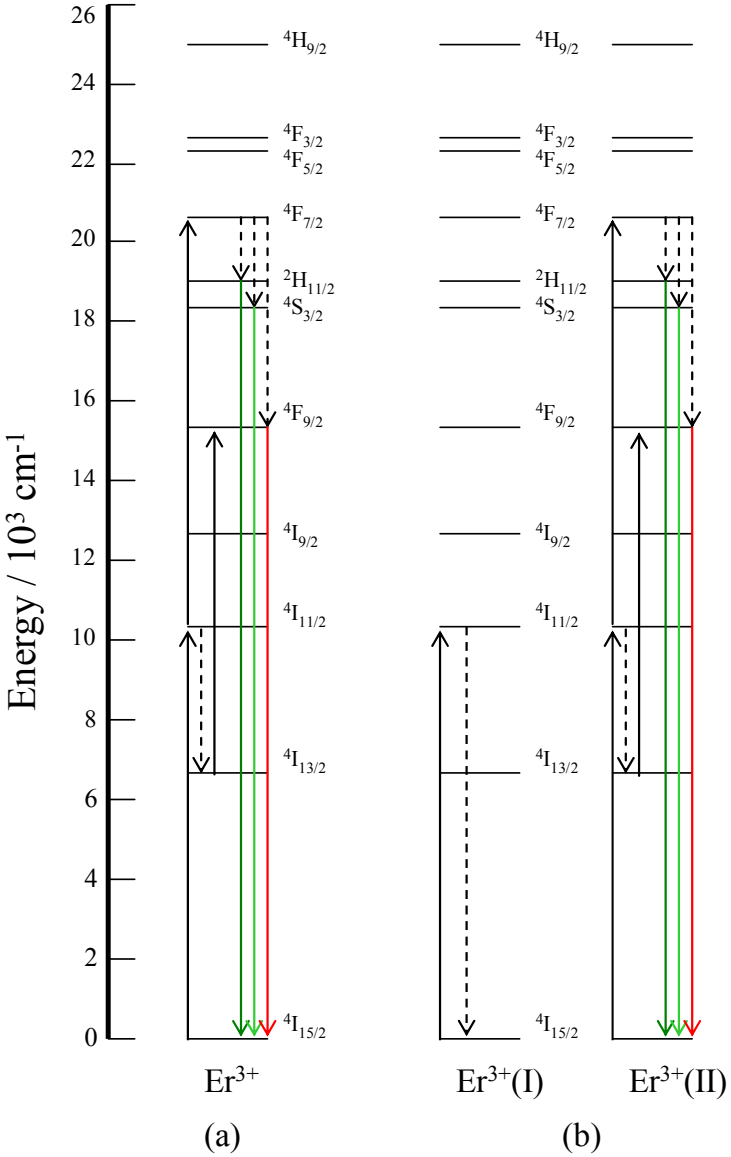

Figure 7 Schematic: (a) ESA and (b) ET UC processes occurring at the $^4I_{11/2}$ and $^4I_{13/2}$ states under 980 nm excitation.

The energy level schematics of the ESA and ET UC processes occurring at the $^4I_{11/2}$ and $^4I_{13/2}$ states along with the luminescence emissions and non-radiative transitions under 980 nm excitation are shown in Figure 7, a and b. In Figure 7a, a single Er^{3+} ion is excited from the $^4I_{15/2}$ ground state to the $^4I_{11/2}$ excited state, via GSA. A second incoming 980 nm photon is then absorbed and excites Er^{3+} to the higher $^4F_{7/2}$ state. ESA is also to known to occur at the $^4I_{13/2}$ state as the result of non-radiative decay from the $^4I_{11/2}$ state after the absorption of the initial photon. A second incoming photon is then absorbed exciting Er^{3+} directly to the $^4F_{9/2}$ state. In the ET process (Figure 7b), two neighboring Er^{3+} ions are simultaneously excited to the $^4I_{11/2}$ intermediate state. From here, one Er^{3+} ion will relax back to its ground state and transfer its energy to the neighboring Er^{3+} ion resulting in direct population of the $^4F_{7/2}$ higher state. Alternatively, one of the Er^{3+} ions can decay to the $^4I_{13/2}$ state where ET from the neighboring Er^{3+} ion results in population of the $^4F_{9/2}$ state. Non-radiative relaxation from the higher $^4F_{7/2}$ excited state results in the population of the $^2H_{11/2}$, $^4S_{3/2}$, and $^4F_{9/2}$ emitting states.

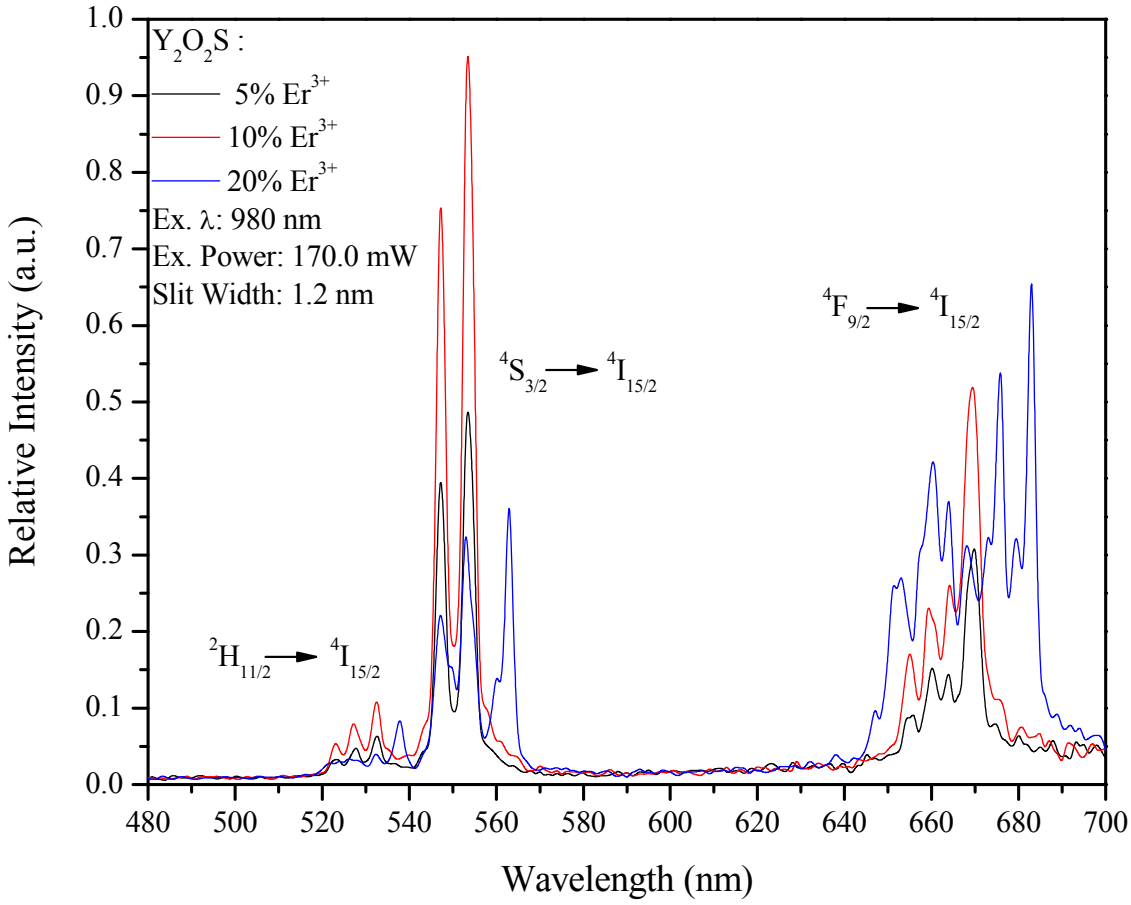

Figure 8 UC emission spectra of Y_2O_2S phosphors doped with 5%, 10% and 20% Er^{3+}.

Figure 8 shows the room temperature UC emission spectra of Y_2O_2S phosphors doped with 5%, 10%, and 20% Er^{3+} under 980 nm excitation operating with an output power of 170 mW. Doubling the Er^{3+} concentration from 5% to 10% showed significant enhancement on the luminescence intensity for both the green and red emission bands. This increase in emission intensity is a result of ET between Er^{3+} atoms in close proximity. The 20% Er^{3+} doped sample exhibited unique spectral broadening of both luminescence bands with additional peak formations previously not seen when subjected

to 808 nm excitation. This is due to incomplete sulfurization of Y_2O_3 and where the spectral profile of the red emission band matches that of the bulk Yb^{3+} and Er^{3+} co-doped Y_2O_3 phosphors. Thus, it is concluded that when doping with higher Er^{3+} concentrations longer reaction times are required in order to complete the sulfurization process.

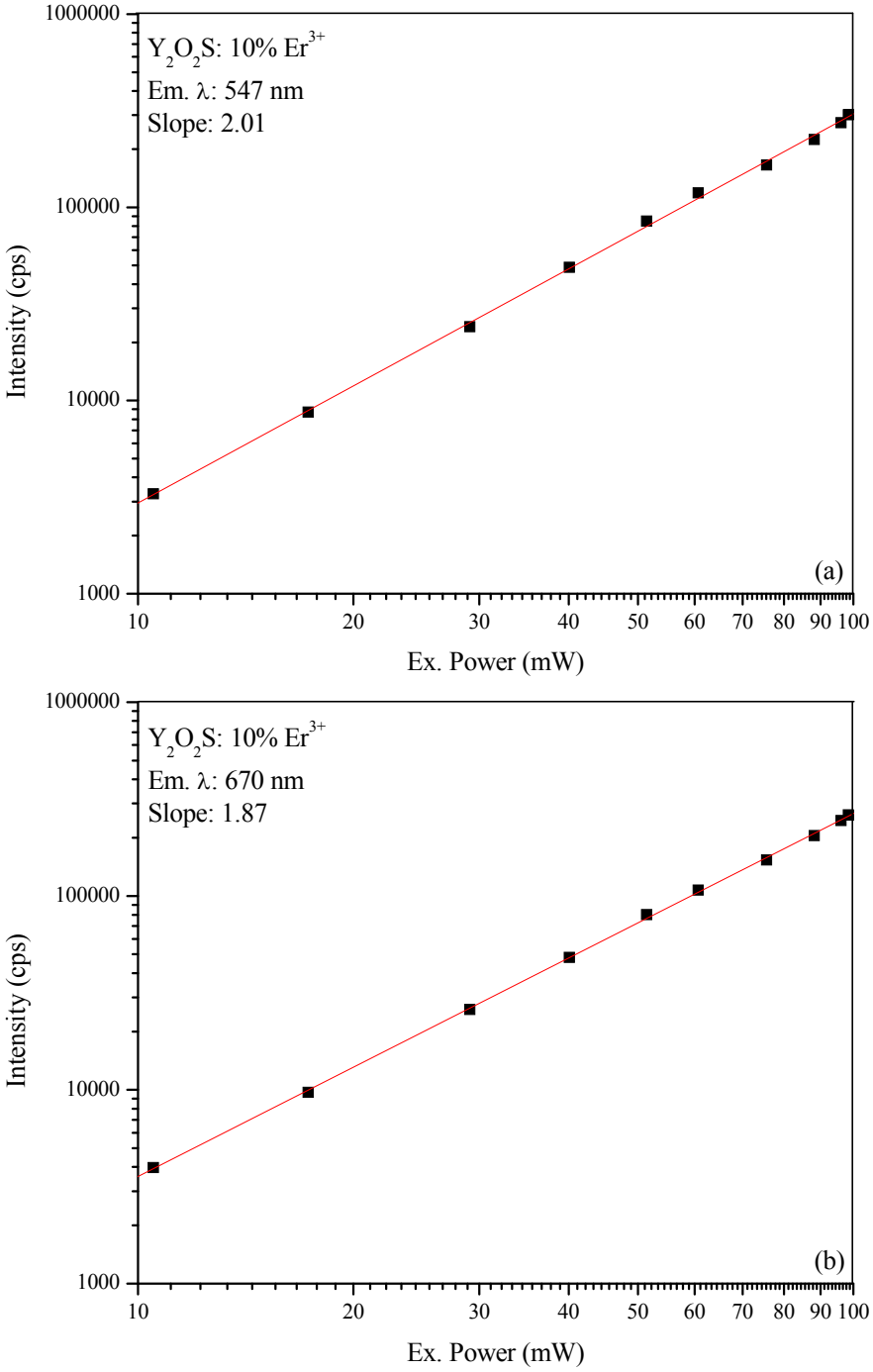

Figure 9 Power dependence of UC intensity of the Y_2O_2S phosphor doped with 10% Er^{3+} monitored at (a) 547 nm, and (b) 670 nm under 980 nm excitation.

Figure 9 shows the power dependence of UC intensity of 10% Er^{3+} doped Y_2O_2S phosphor monitored at (a) 547 nm and (b) 670 nm. From the power dependence plots, the UC emissions monitored at 547 nm and 670 nm required 2.01 and 1.87 photons for the 10% Er^{3+} doped sample. It is interesting to note that the power dependence measurements monitoring the 547 and 670 nm emission peaks showed that singly doped Er^{3+} Y_2O_2S phosphors, independent of concentration, have the same linear power dependence under both 808 and 980 nm excitation where the number of NIR pumping photons required to generate both the 547 and 670 nm emission peaks remained the same, respectively.

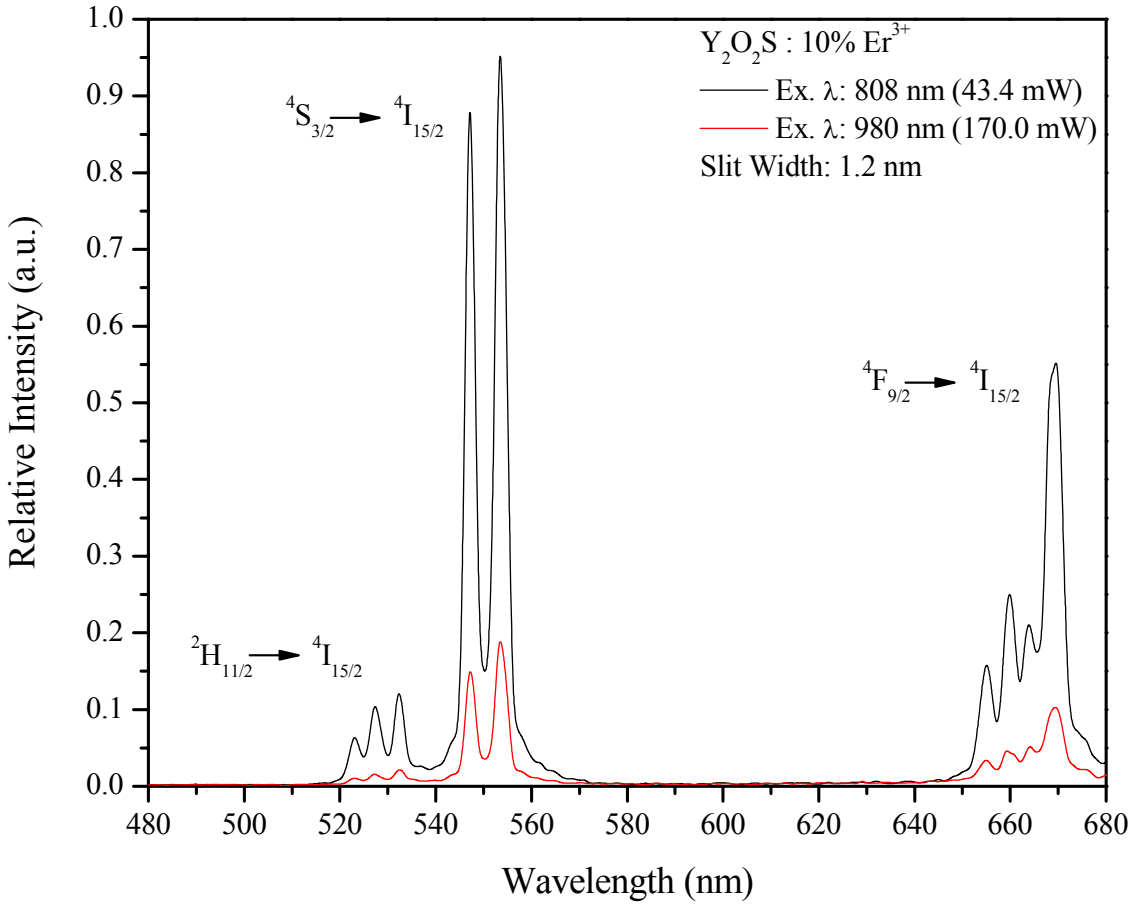

Figure 10 UC emission spectra of Y_2O_2S: 10% Er^{3+} phosphors under 808 and 980 nm excitation.

Figure 10 shows the room temperature UC emission spectra of the 10% Er^{3+} doped Y_2O_2S phosphors under 808 and 980 nm excitation. The difference in the emission intensities suggests that the UC process in singly doped Er^{3+} Y_2O_2S phosphors is much more efficient under 808 than 980 nm excitation which is not at all surprising. It is well known, that without the presence of Yb^{3+} acting as a sensitizer that the efficiency of the UC process ultilizing 980 nm excitation is rather inefficient. In addition to having the same power dependence upon 808 and 980 nm excitation, Figure 10 also shows that the

spectral profiles of the UC emission bands remain the same. Thus, the only major difference is how this process is occurring mechanistically and the subtle differences in the UC mechanisms is more obvious when directly compared and is shown in Figure 11.

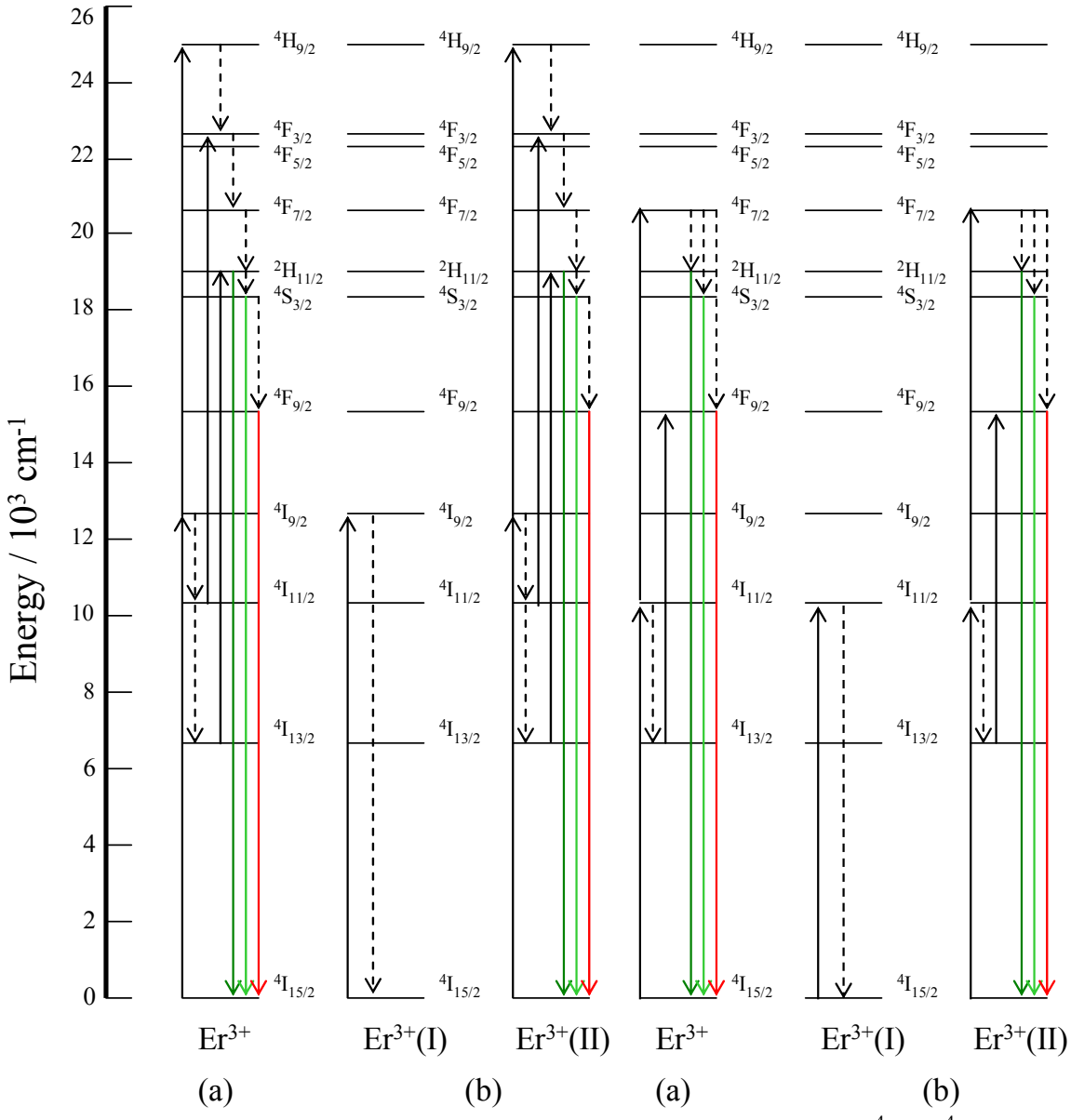

Figure 11 Schematic: (a) ESA and (b) ET UC processes occurring at the $^4I_{13/2}$, $^4I_{11/2}$, and $^4I_{9/2}$ states under 808 nm (left) and $^4I_{11/2}$, and $^4I_{9/2}$ states under 980 nm excitation (right).

Figure 11 shows the schematic illustrations of the ESA and ET UC processes occurring at the $^4I_{13/2}$, $^4I_{11/2}$, and $^4I_{9/2}$ states under 808 nm (left) and $^4I_{11/2}$, and $^4I_{9/2}$ states under 980 nm excitation (right). When compared side by side the slight differences in the UC mechanisms become more apparent and can be clearly established. The non-radiative $^4I_{9/2} \rightarrow {}^4I_{11/2}$, $^4I_{13/2}$ and $^4I_{11/2} \rightarrow {}^4I_{13/2}$ transitions which can occur following GSA of an 808 nm photon, will not affect the population of the higher green and red emitting states. Depending on which excited state Er^{3+} is in following GSA and considering the non-radiative transitions, ESA or ET will either directly populate the $^2H_{11/2}$ emitting state from the $^4I_{9/2}$ state or indirectly through series of non-radiative transitions from the higher $^4H_{9/2}$ or $^4F_{3/2}$, $^4F_{5/2}$ states. As a result, the $^2H_{11/2}$ emitting state is solely responsible for the population of the $^4S_{3/2}$ and $^4F_{9/2}$ emitting states and therefore essential for UC under 808 nm excitation. Immediately following GSA of a 980 nm photon, the ESA or ET UC processes which are known to occur at both the $^4I_{11/2}$ and the $^4I_{13/2}$ intermediate states will result in different wavelengths to be emitted. ESA or ET from the $^4I_{11/2}$ state results in indirect population of the $^2H_{11/2}$, $^4S_{3/2}$, and $^4F_{9/2}$ emitting states through non-radiative relaxation from the higher $^4F_{7/2}$ state and as a result both green and red emissions can be produced. However, ESA or ET from the $^4I_{13/2}$ state as a result of the non-radiative $^4I_{11/2} \rightarrow {}^4I_{13/2}$ transition following GSA, directly populates the $^4F_{9/2}$ state only and as a result only a red emission will be produced. This alternate pathway decreases the likelihood of populating the higher $^2H_{11/2}$ and $^4S_{3/2}$ emitting states and as a result the efficiency of the

980 nm UC process with respect to the green emissions corresponding to the radiative $^2H_{11/2}$, $^4S_{3/2} \rightarrow {}^4I_{15/2}$ transitions will be decreased.

It is noteworthy to mention that the UC luminescence properties regarding spectral emission profiles, dependence on the excitation power, and mechanisms for singly doped Er^{3+} Y_2O_2S phosphors occurring under 808 and 980 nm excitation has not been directly compared in the established literature and is reported here for the first time.

3.2.2 $Y_2O_2S:Yb^{3+}$, Er^{3+} Phosphors under 980 nm Excitation

3.2.2.1 Fixing Yb^{3+} and Increasing Er^{3+}

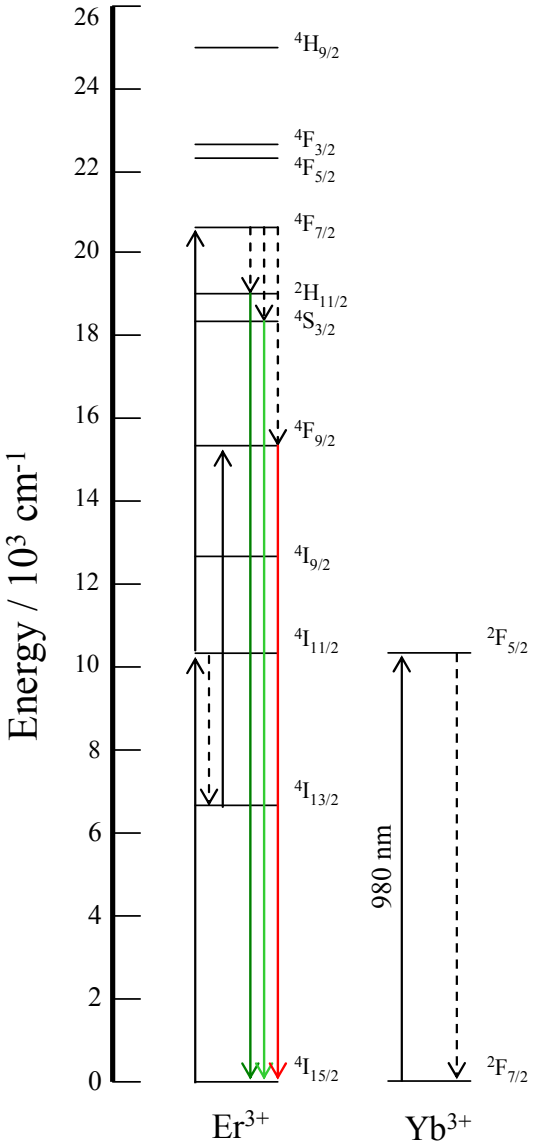

Figure 12 Schematic of the ET UC process from Yb^{3+} to Er^{3+}occurring at the $^4I_{11/2}$ and $^4I_{13/2}$ states under 980 nm excitation.

The energy level schematic of the resonant ET UC process occurring at the $^4I_{11/2}$ and $^4I_{13/2}$ states along with the luminescence emissions and non-radiative transitions under 980 nm excitation are shown in Figure 12. Upon 980 nm excitation the first Yb^{3+} ion transfers its energy to the ground state of Er^{3+} exciting it to the $^4I_{11/2}$ state. A second excited Yb^{3+} ion then relaxes and transfers its energy to the same excited neighboring Er^{3+} atom resulting in the population of the $^4F_{7/2}$ state. Non-radiative relaxation from the higher $^4F_{7/2}$ state results in the population of the $^2H_{11/2}$, $^4S_{3/2}$ and $^4F_{9/2}$ emitting states. However, immediately following the first initial ET from Yb^{3+}, Er^{3+} can non-radiatively decay to the $^4I_{13/2}$ state where now the second resonant ET from Yb^{3+} will result in the population of the $^4F_{9/2}$ emitting state only.

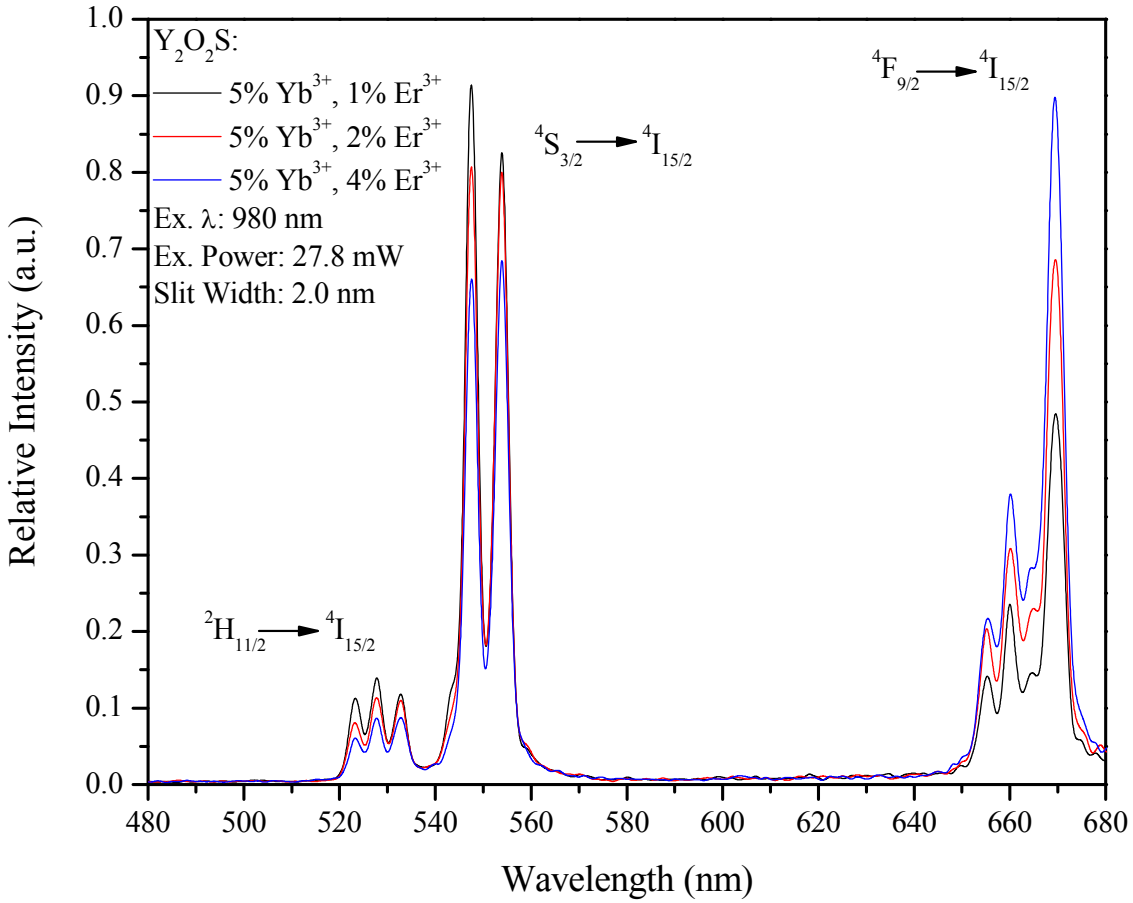

Figure 13 UC emission spectra of Y_2O_2S phosphors doped with 5% Yb^{3+}, X% Er^{3+}, where X ranges from 1.0 - 4.0.

Figure 13 shows the room temperature UC emission spectra of Y_2O_2S phosphors doped with 5% Yb^{3+} and X% Er^{3+}, where X ranges from 1.0 - 4.0 under 980 nm excitation operating with an output power of 27.8 mW. Increasing the Er^{3+} concentration in the fixed Yb^{3+} doped phosphors lead to an increase in the intensity of the red emission band while subsequently lead to a decrease in the intensity of the green emission bands. It is important to note that the emission pathways corresponding to the $(^2H_{11/2})^4S_{3/2}$, $^4F_{9/2} \rightarrow {}^4I_{15/2}$ transitions are directly affected and dependent upon the Er^{3+} concentration. Higher

Er^{3+} concentrations lead to higher tendency for interactions between neighboring Er^{3+} ions. Therefore, it has been proposed by several authors studying Yb^{3+} and Er^{3+} co-doped nanocrystalline Y_2O_3 phosphors that the non-radiative $^4F_{7/2} \rightarrow {}^4F_{9/2}$ transition not only results in a red emission around 660 nm but also directly populates the $^4F_{9/2}$ state of a neighboring excited Er^{3+} ion from the $^4I_{11/2}$ state via the $^4F_{7/2}$ Er^{3+}(I) + $^4I_{11/2}$ Er^{3+}(II) → $^4F_{9/2}$ Er^{3+}(I) + $^4F_{9/2}$ Er^{3+}(II) cross-relaxation mechanism shown below in Figure 14.[3], [4], [8], [14] It should be noted that when the Er^{3+} concentration reached 4% the intensity of the red emission band became more intense than the intensity of the green emission band. The decrease in the green emission intensity observed when the Er^{3+} concentration is increased is not a result of concentration quenching but could possibly be, to a lesser extent, a result of this cross-relaxation mechanism. Although, this would explain the significant increase in the intensity of red emission observed, cross-relaxation between Er^{3+} ions is highly unlikely due to the low dopant concentration. A simpler explanation for the observable changes in the intensities would be that when the Er^{3+} concentration reaches nearly that of Yb^{3+} the efficiency of the non-radiative $^4F_{7/2} \rightarrow {}^4F_{9/2}$ and $^4I_{13/2} \rightarrow {}^4I_{15/2}$ transitions becomes increased.

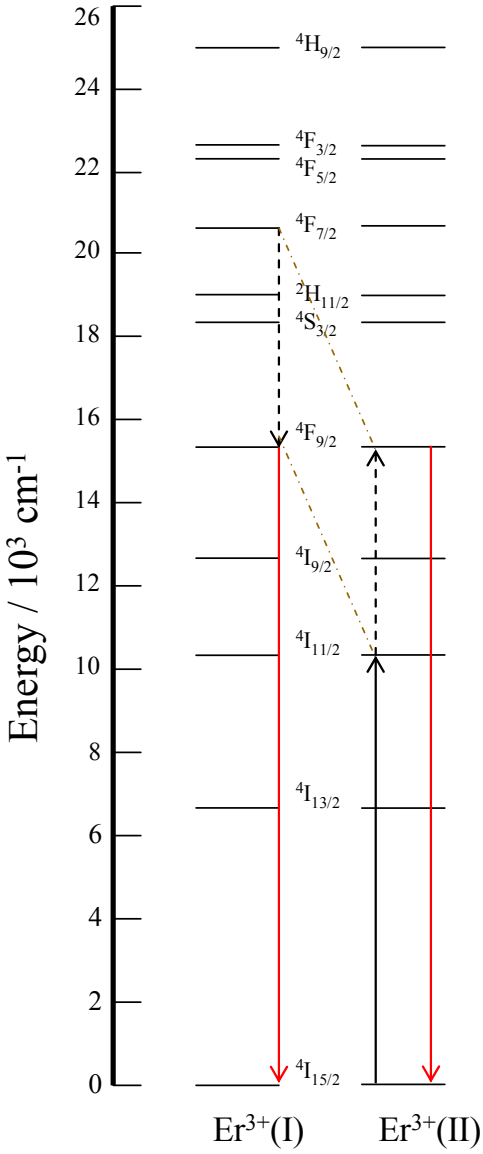

Figure 14 Schematic: $^4F_{7/2}Er^{3+}(I) + {}^4I_{11/2}Er^{3+}(II) \rightarrow {}^4F_{9/2}Er^{3+}(I) + {}^4F_{9/2}Er^{3+}(II)$ cross-relaxation process possibly responsible for the $^4F_{9/2}$ state under 980 nm excitation.

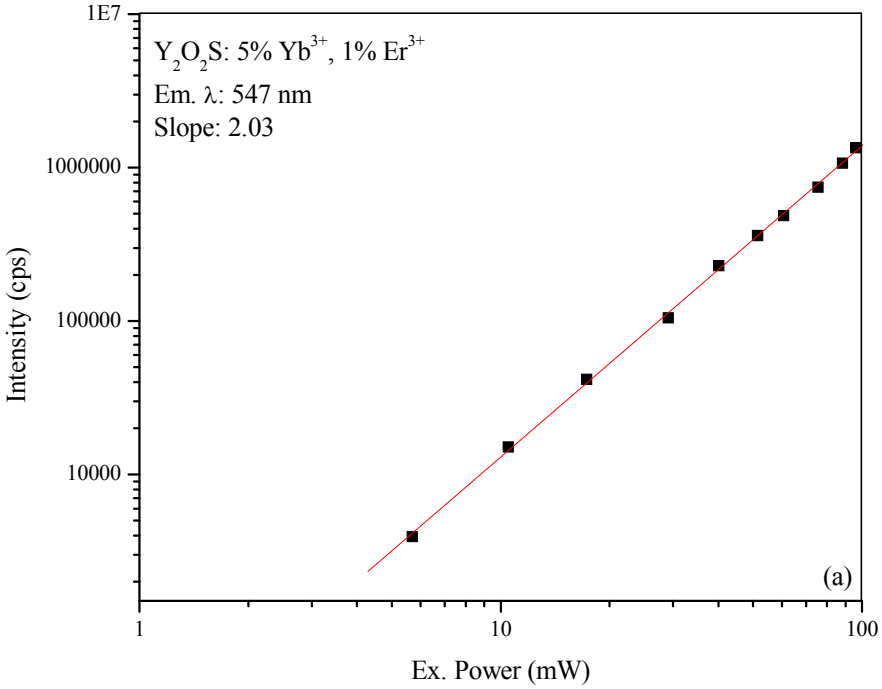
1E7
1000000
100000
10000
Intensity (cps)
Y_2O_2S: 5% Yb^{3+}, 1% Er^{3+}
Em. λ: 547 nm
Slope: 2.03
(a)
1
10
100
Ex. Power (mW)

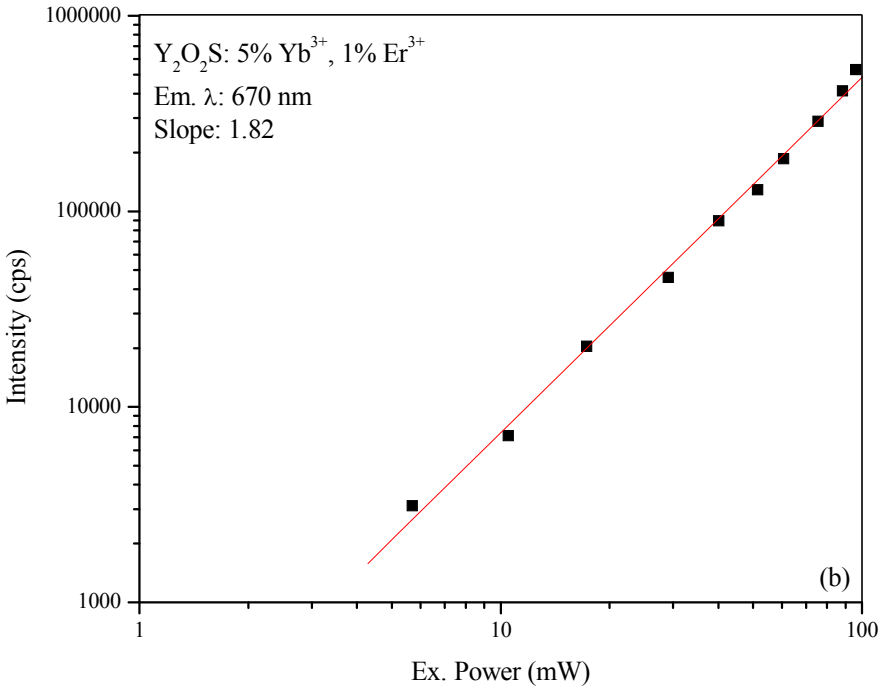
1000000
100000
10000
1000
Intensity (cps)
Y_2O_2S: 5% Yb^{3+}, 1% Er^{3+}
Em. λ: 670 nm
Slope: 1.82
(b)
1
10
100
Ex. Power (mW)

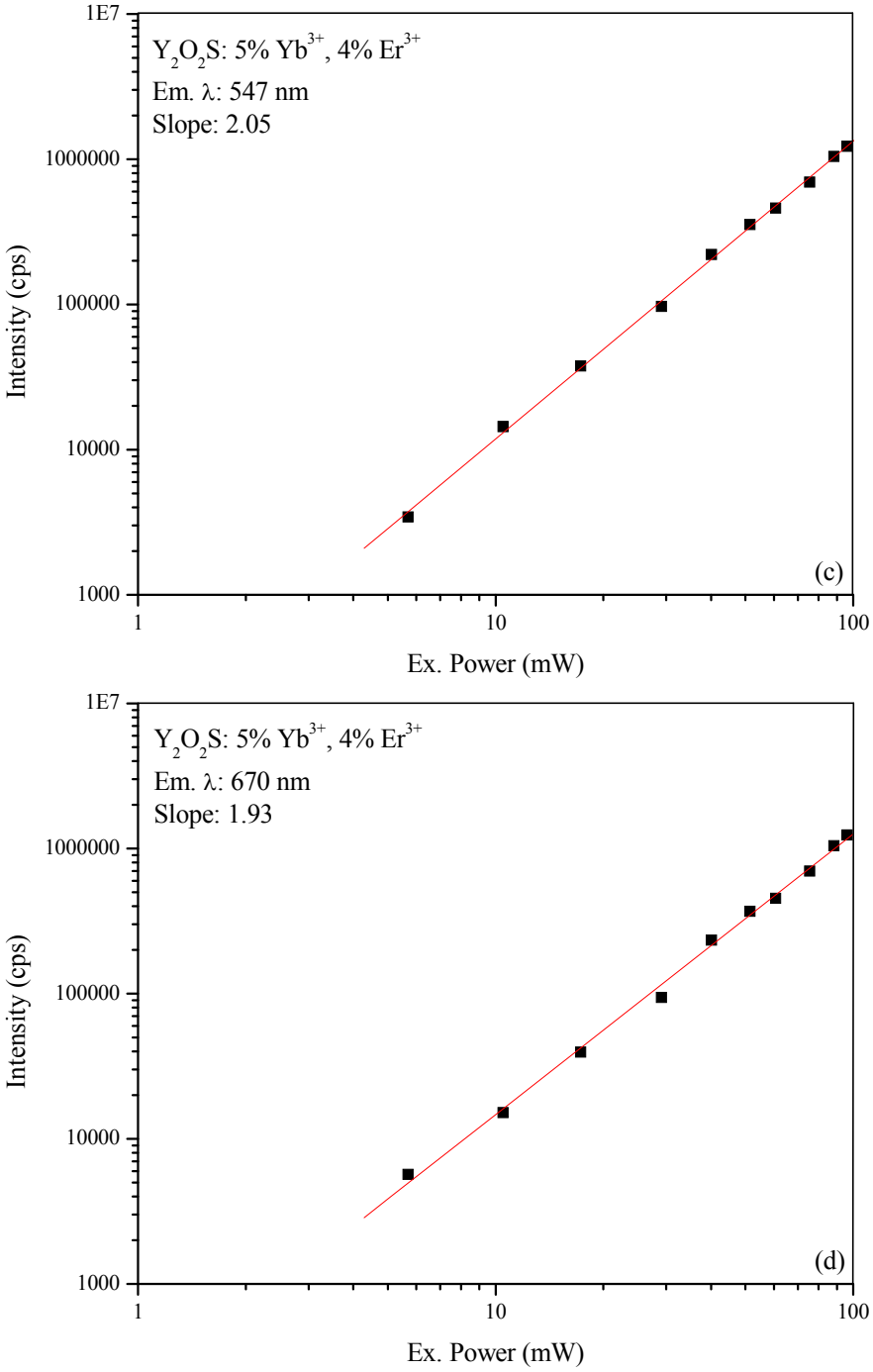

Figure 15 Power dependence of UC intensity of Y_2O_2S: 5%Yb^{3+} phosphors doped with 1% Er^{3+} and 4% Er^{3+} monitored at (a), (c) 547 nm, and (b), (d) 670 nm under 980 nm excitation.

Figure 15 shows the power dependence of UC intensity of Y_2O_2S phosphors doped with (a), (b) 5% Yb^{3+}, 1% Er^{3+}, and (c), (d) 5% Yb^{3+}, 4% Er^{3+}. From the power dependence plots, the UC emissions monitored at 547 nm and 670 nm required 2.03 and 1.82 photons for the 1% Er^{3+} doped sample and 2.05 and 1.93 photons for the 4% Er^{3+} doped sample. Ultimately, this rules out the possibility of this cross-relaxation mechanism since the number of NIR pumping photons required to populate the $^4S_{3/2}$ and $^4F_{9/2}$ emitting states for both the 1% and 4% Er^{3+} doped sample remained the same, respectively. Therefore, it is most likely that the changes in the intensity of the green and red emission bands observed in the UC emission spectra are in fact due to the non-radiative $^4F_{7/2} \rightarrow {}^4F_{9/2}$ and $^4I_{13/2} \rightarrow {}^4I_{15/2}$ transitions which become more predominant as the concentration of Er^{3+} is increased.

3.2.2.2 Fixing Er^{3+} and Increasing Yb^{3+}

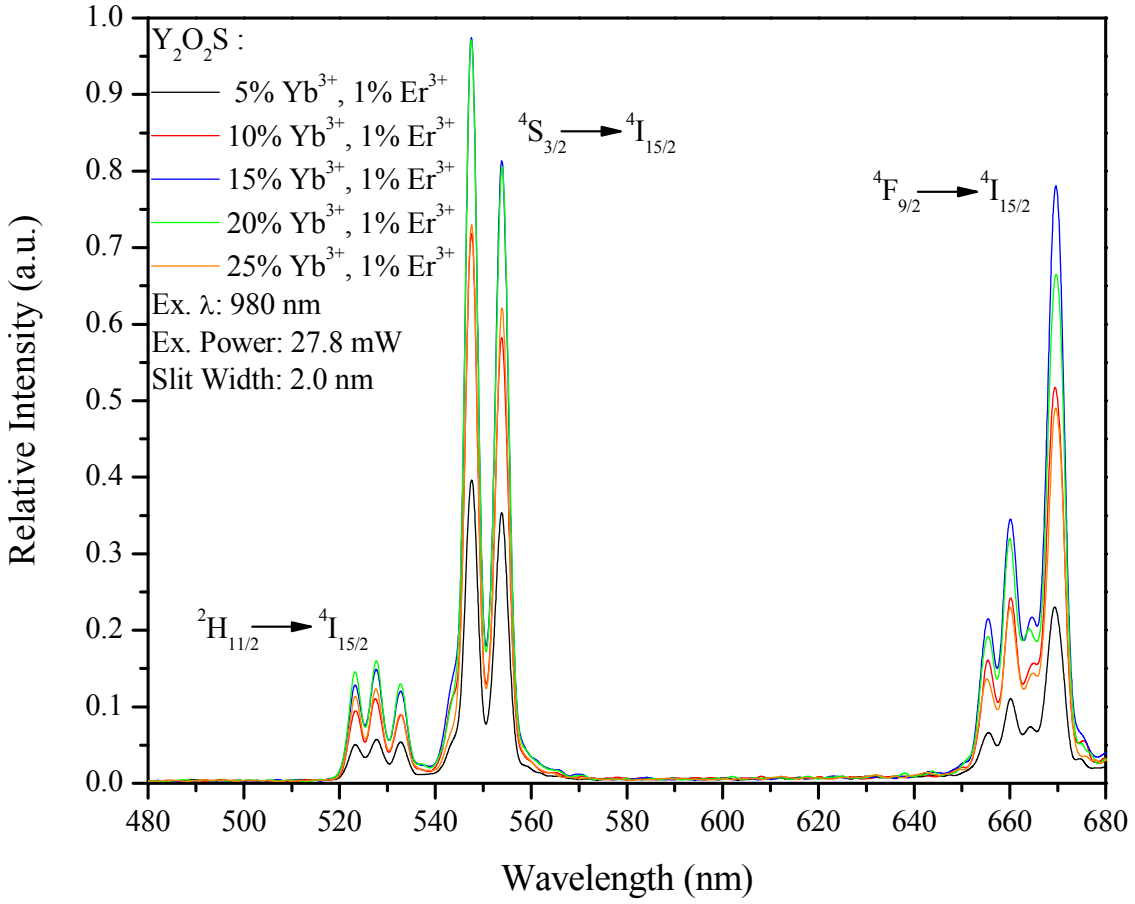

Figure 16 UC emission spectra of Y_2O_2S phosphors co-doped with X% Yb^{3+}, 1% Er^{3+}, where X ranges from 5.0 - 25.0.

Figure 16 shows the room temperature UC emission spectra of Y_2O_2S phosphors doped with X% Yb^{3+}, 1% Er^{3+}, where X is incrementally increased by 5% from 5.0 - 25.0 under 980 nm excitation operating with an output power of 27.8 mW. Increasing the Yb^{3+} concentration in the fixed Er^{3+} doped phosphors from 5% to 15% caused the intensity of the green and red emission bands corresponding to the $(^2H_{11/2})^4S_{3/2}$, $^4F_{9/2} \rightarrow {}^4I_{15/2}$ transitions to increase significantly. However, when the Yb^{3+} concentration was increased

to 20% only the intensity of the red emission was decreased whereas the green emission intensity remained unaffected, respectively. The $^4I_{13/2}$ state plays an important role in helping generate the red luminescence emission by directly populating the $^4F_{9/2}$ emitting state from a second ET from Yb^{3+}. Increasing the Yb^{3+} concentration to 20% reduced the likelihood for the non-radiative $^4I_{11/2} \rightarrow {}^4I_{13/2}$ transition to occur as well as the non-radiative $^4F_{7/2} \rightarrow {}^4F_{9/2}$ transition which resulted in a decrease in red luminescence intensity. This also explains why the green luminescence intensity did not exhibit the same effect and remained unchanged, respectively. It is necessary to note that when the Yb^{3+} concentration reaches 25% the emission intensity diminishes as a result of concentration quenching where energy is back transferred to the Yb^{3+} ions.

3.2.2.3 Increasing Yb^{3+} and Er^{3+}, Maintaining a 5:1 Mol Ratio

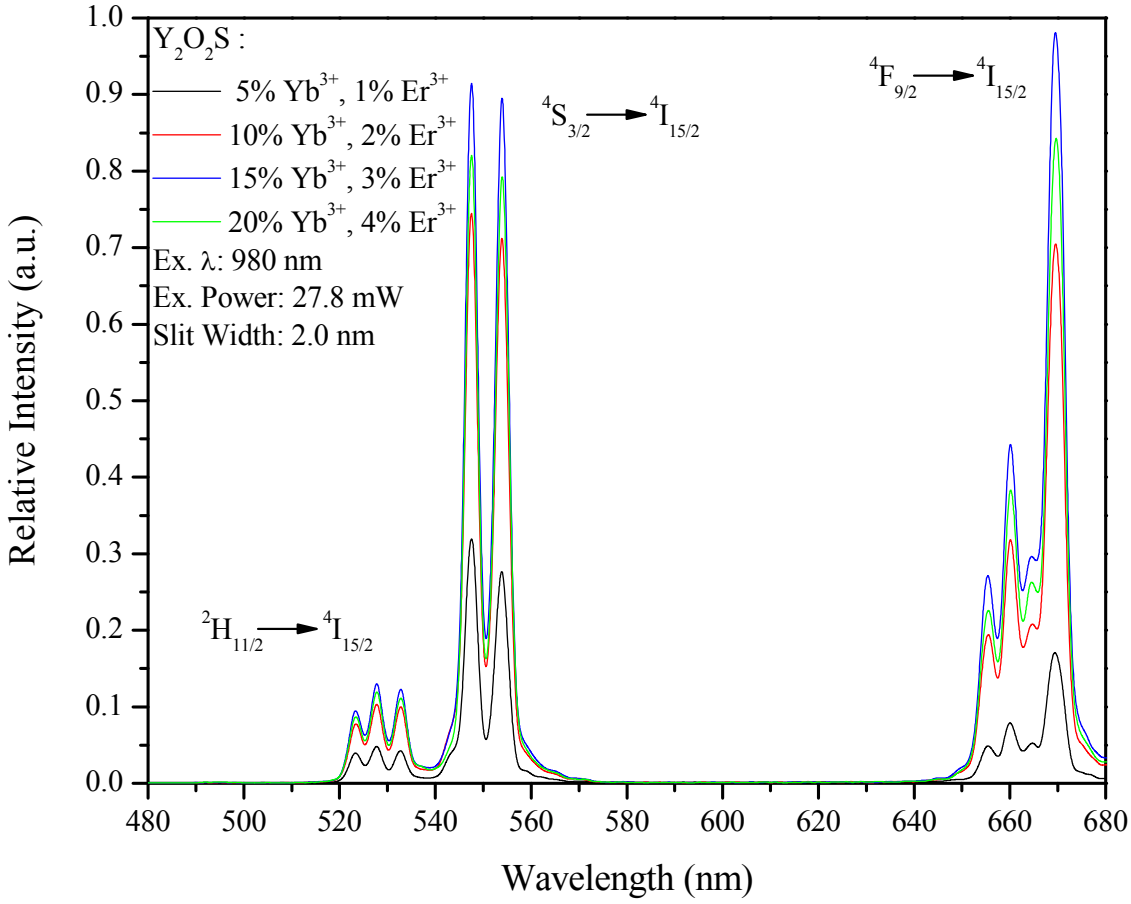

Figure 17 UC emission spectra of Y_2O_2S phosphors co-doped with a fixed 5:1 Yb^{3+} to Er^{3+} mol ratio with increasing concentrations.

Figure 17 shows the room temperature UC emission spectra of Y_2O_2S phosphors doped with different concentrations of Yb^{3+} and Er^{3+}, while maintaining a 5:1 mol ratio under 980 nm excitation operating with an output power of 27.8 mW. Increasing the concentration of Yb^{3+} and Er^{3+} caused the intensity of the green and red emission bands corresponding to the $(^2H_{11/2})^4S_{3/2}$, $^4F_{9/2} \rightarrow {}^4I_{15/2}$ transitions to increase significantly. However, when a 5:1 mol ratio of 20% Yb^{3+} and 4% Er^{3+} is incorporated into the Y_2O_2S

host lattice the intensity of both the green and red emissions decreased as a result of concentration quenching.

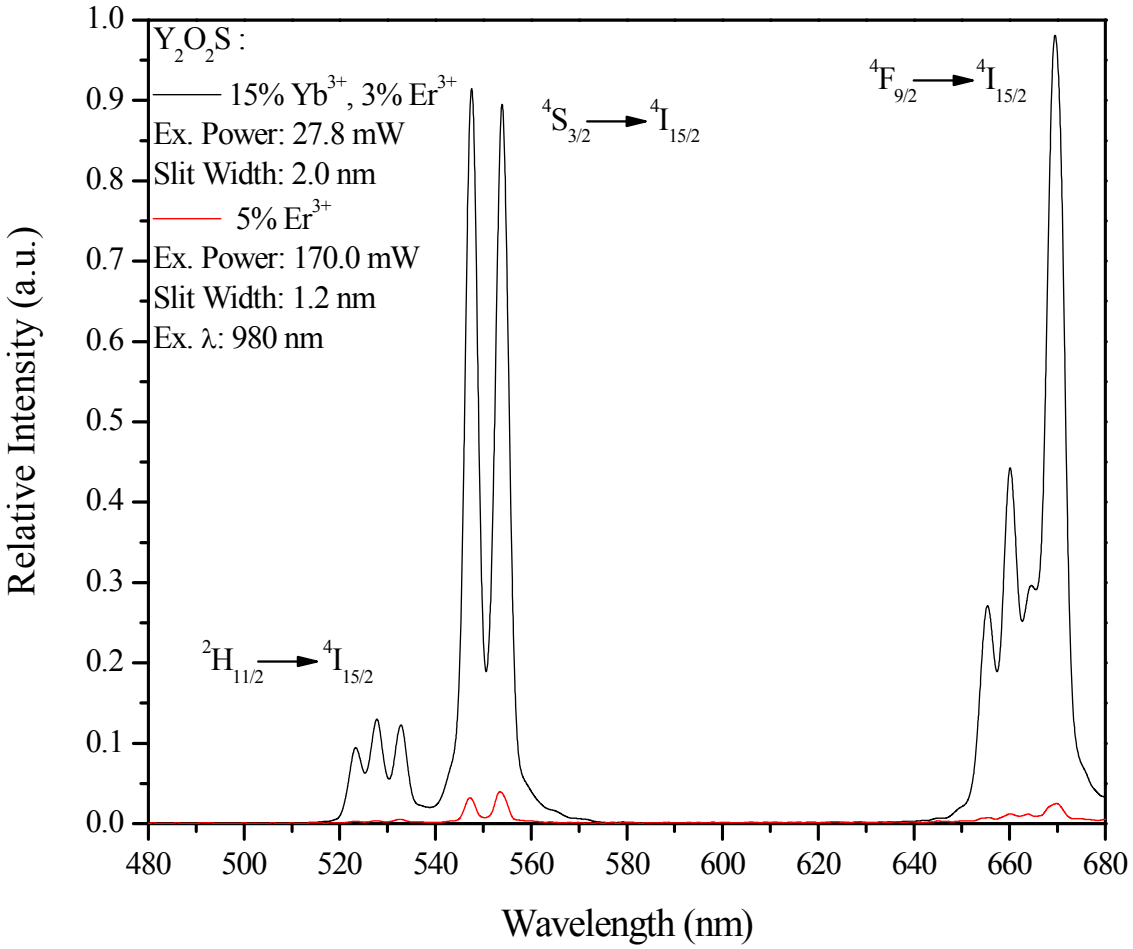

Figure 18 UC emission spectra of 15% Yb^{3+}, 3% Er^{3+} co-doped and 5% Er^{3+} doped Y_2O_2S phosphors under 980 nm excitation.

Figure 18 shows the room temperature UC emission spectra of Y_2O_2S phosphors co-doped with 15% Yb^{3+}, 3% Er^{3+} and doped with 5% Er^{3+}. A significant enhancement in the UC luminescence intensity for both the green and red emission bands is clearly observed. It is clear from the emission spectra that co-doping Er^{3+} with Yb^{3+} significantly

increases the efficiency of the 980 nm UC process as it is well known that the excited state of Yb^{3+} possesses a much larger absorption cross-section than the $^4I_{11/2}$ excited state of Er^{3+}.[3] The increase in the UC efficiency is due solely to the well-defined spectral overlap between (Yb^{3+}) $^2F_{5/2} \rightarrow {}^2F_{7/2}$ NIR emission band and (Er^{3+}) $^4I_{11/2} \leftarrow {}^4I_{15/2}$ absorption band. It is concluded from the emission spectra, that the majority of visible light generated upon 980 nm excitation is due to the resonant ET from Yb^{3+} to Er^{3+} since the luminescence signal of the 5% Er^{3+} doped Y_2O_2S phosphors is negligible in comparison.

3.2.3 1560 nm Excitation

3.2.3.1 $Y_2O_2S:Er^{3+}$ Phosphors

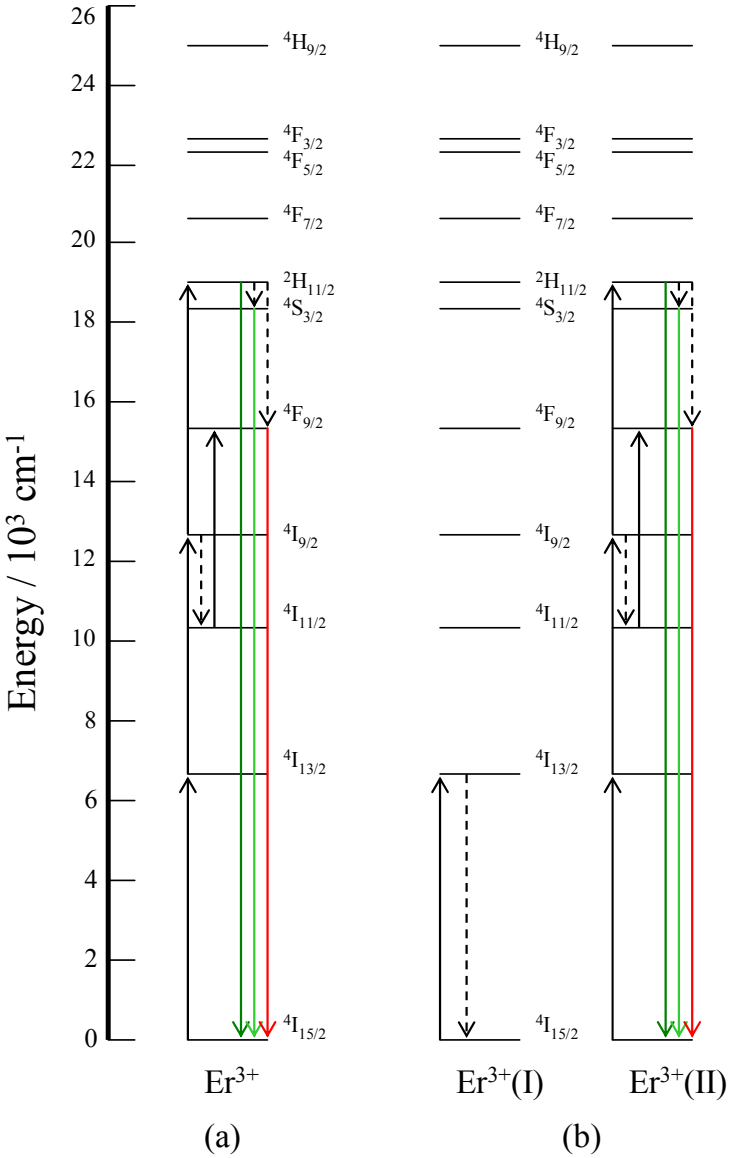

Figure 19 Schematic: (a) ESA and (b) ET UC processes occurring at the $^4I_{13/2}$, $^4I_{9/2}$, and $^4I_{11/2}$ states under 1560 nm excitation.

The energy level schematic of the ESA and ET UC processes occurring at the $^4I_{13/2}$, $^4I_{9/2}$, and $^4I_{11/2}$ states along with the luminescence emissions and non-radiative transitions under 1560 nm excitation are shown in Figure 19, a and b. In the ESA process (Figure 19a), a single Er^{3+} ion is excited from the $^4I_{15/2}$ ground state to the $^4I_{13/2}$ excited state. A second 1560 nm photon then excites Er^{3+} from the $^4I_{13/2}$ state to the $^4I_{9/2}$ state where finally a third incoming photon excites Er^{3+} to the $^2H_{11/2}$ emitting state. ESA is also known to occur at the $^4I_{11/2}$ state as the result of non-radiative decay from the $^4I_{9/2}$ state after the absorption of the second incoming photon. A third incoming photon is then absorbed and directly excites Er^{3+} to the $^4F_{9/2}$ emitting state. In the ET process (Figure 19b), Er^{3+} ions are simultaneously excited to the $^4I_{13/2}$ state. From here, multiple Er^{3+} ions will act as sensitizers, relaxing back to the $^4I_{15/2}$ ground state and transfer their energy to the neighboring activator Er^{3+} ion resulting in the direct population of the $^2H_{11/2}$ emitting state through a two-step ET process. Alternatively, the activating Er^{3+} ion can non-radiatively decay to the $^4I_{11/2}$ state where ET from the neighboring Er^{3+} ion results in the direct population of the $^4F_{9/2}$ emitting state.[24] Non-radiative transitions from the higher $^2H_{11/2}$ emitting state result in the population of the $^4S_{3/2}$ and $^4F_{9/2}$ emitting states where spin-allowed transitions back to the $^4I_{15/2}$ ground state result in green emissions around 530 and 550 nm and red emissions around 660 - 670 nm.

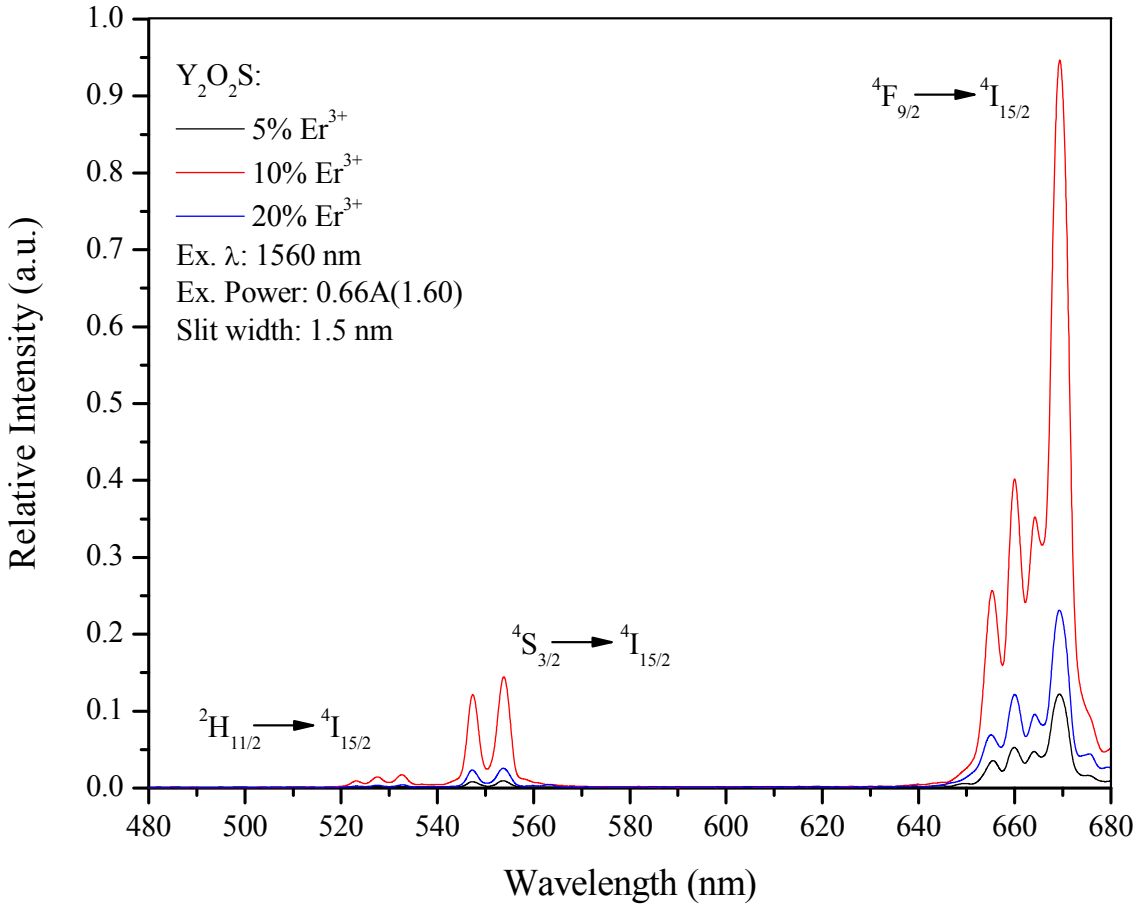

Figure 20 UC emission spectra of Y_2O_2S phosphors doped with 5%, 10%, and 20% Er^{3+}.

Figure 20 shows the room temperature UC emission spectra of Y_2O_2S phosphors doped with 5%, 10%, and 20% Er^{3+} under 1560 nm excitation. Doubling the Er^{3+} concentration from 5% to 10% showed significant enhancement on the luminescence intensity for both the green and red emission bands. This increase in emission intensity is a result of ET between Er^{3+} ions in close proximity. When doped with 20% Er^{3+}, the intensity of all emission bands decreased considerably as result of concentration quenching.

3.2.3.2 $Y_2O_2S:Yb^{3+}, Er^{3+}$ Phosphors

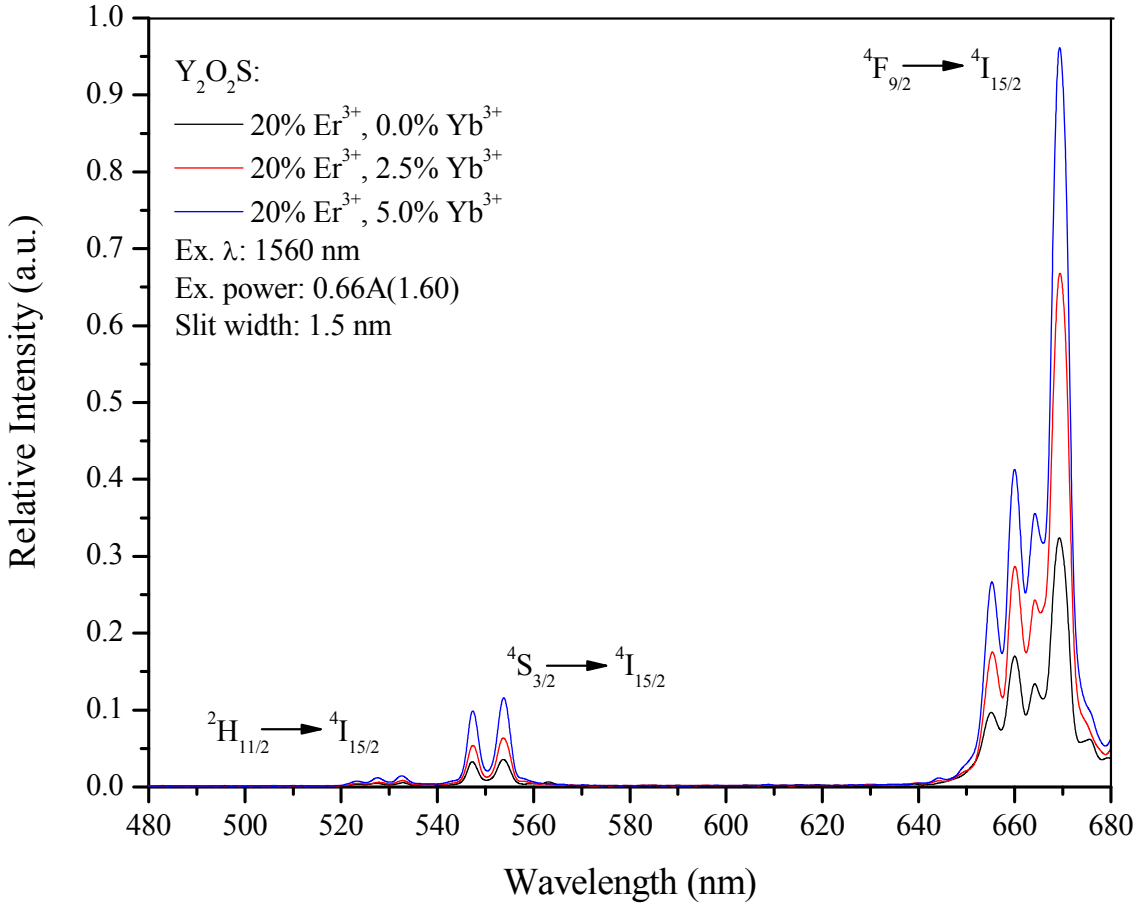

Figure 21 UC emission spectra of Y_2O_2S phosphors co-doped with 20% Er^{3+} and X% Yb^{3+}, where X ranges from 0.0 - 5.0.

Figure 21 shows the room temperature UC emission spectra of Y_2O_2S phosphors doped with 20% Er^{3+}, X% Yb^{3+}, where X is incrementally increased by 2.5% from 0.0 - 5.0 under 1560 nm excitation. Increasing the Yb^{3+} concentration in the fixed Er^{3+} doped phosphors from 0% to 5% caused the intensity of the red emission band corresponding to $^4F_{9/2} \rightarrow {}^4I_{15/2}$ transition to increase significantly whereas the intensity of the green emission consistent with the $(^2H_{11/2})^4S_{3/2} \rightarrow {}^4I_{15/2}$ transition was only slightly enhanced.

Therefore, co-doping Er^{3+} with Yb^{3+} has a direct effect on the $^4F_{9/2}$ emitting state. Two different mechanisms believed to be the most plausible are proposed, schematically shown, and addressed in detail.

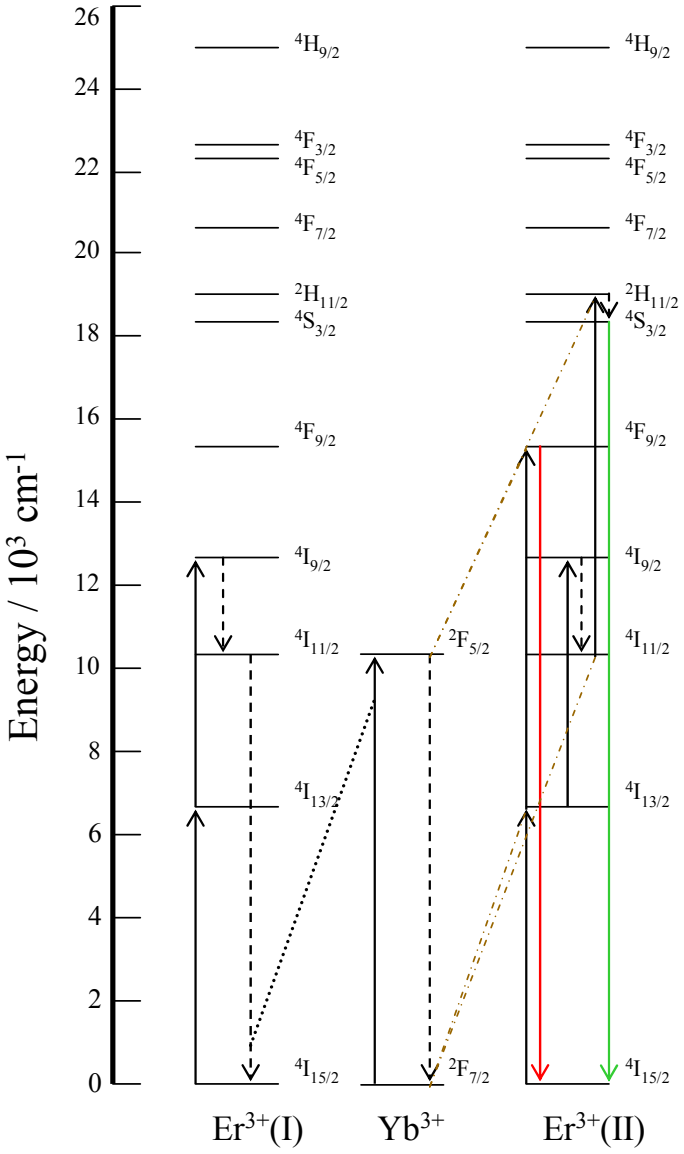

Figure 22 Schematic:
(1) $^4I_{11/2}Er^{3+}(I) + {}^2F_{7/2}Yb^{3+} \rightarrow {}^4I_{15/2}Er^{3+}(I) + {}^2F_{5/2}Yb^{3+}$
(2) $^2F_{5/2}Yb^{3+} + {}^4F_{13/2}Er^{3+}(II) \rightarrow {}^2F_{7/2}Yb^{3+} + {}^4F_{9/2}Er^{3+}(II)$ ET process possibly responsible for the $^4F_{9/2}$ state under 1560 nm excitation.

In the first case (Figure 22), after a two-step ET process from neighboring Er^{3+} ions, non-radiative relaxation from the $^4I_{11/2} \rightarrow {}^4I_{15/2}$ transition directly excites Yb^{3+} to the

$^2F_{5/2}$ state. From here, Yb^{3+} will relax, transfer its energy and directly excite a neighboring Er^{3+} ion in the $^4I_{13/2}$ intermediate excited state to the $^4F_{9/2}$ emitting state.

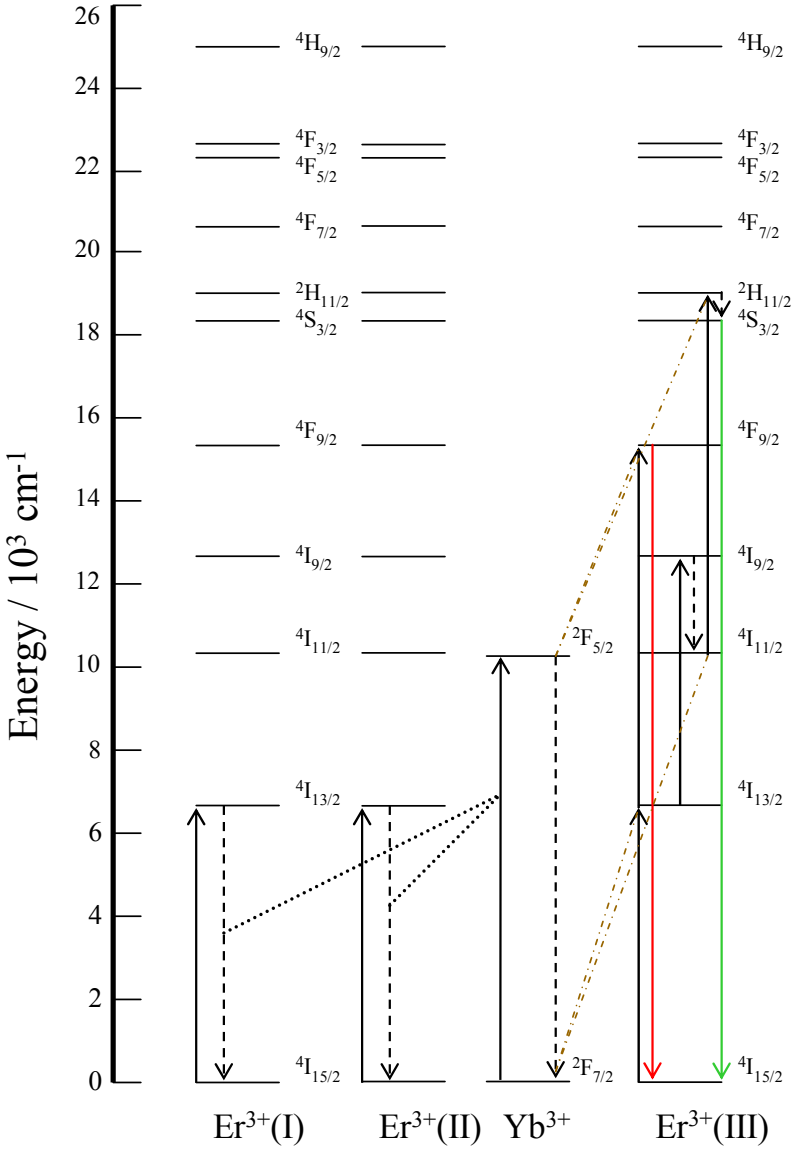

Figure 23 Schematic:
(1) $^4I_{13/2}[Er^{3+}(I), (II),(III)] + {}^2F_{7/2}Yb^{3+} \rightarrow {}^4I_{15/2}[Er^{3+}(I), (II)] + {}^2F_{5/2}Yb^{3+}$
(2) $^2F_{5/2}Yb^{3+} + {}^4I_{13/2}Er^{3+}(III) \rightarrow {}^2F_{7/2}Yb^{3+} + {}^4F_{9/2}Er^{3+}(III)$ cooperative sensitization ET process possibly responsible for the $^4F_{9/2}$ state under 1560 nm excitation.

In the second case (Figure 23) known as cooperative sensitization ET, two individual Er^{3+} ions undergo GSA upon 1560 nm excitation exciting both of them into the $^4I_{13/2}$ state. Simultaneous non-radiative relaxation back to the $^4I_{15/2}$ ground state will directly excite a neighboring Yb^{3+} ion to the $^2F_{5/2}$ excited state where the energy that is being transferred by the cooperative sensitization process is at an energy resonant with the sum of the two excitation energies overlaps well with $^4I_{5/2} \leftarrow {}^4I_{7/2}$ absorption band of Yb^{3+}. Immediately following GSA of 1560 nm photon by a neighboring Er^{3+} ion, Yb^{3+} will then relax and transfer its energy to the same neighboring Er^{3+} ion resulting in direct population of the $^4F_{9/2}$ emitting state.

Rather than the usual consecutive three-photon excitation process that occurs from Er^{3+} only, the incorporation of Yb^{3+} creates a second, more efficient pathway for populating the $^4F_{9/2}$ red emitting state. It is noteworthy to mention that the intensity of the red emission in a 20% Er^{3+} doped sample that earlier exhibited concentration quenching (Figure 21) was significantly enhanced by co-doping with Yb^{3+}.

Unfortunately, the power dependence measurements utilizing 1560 nm excitation will not be reported since this wavelength extends beyond the wavelength range of the power meter which is 1100 nm.

3.3 Conclusions

In conclusion, bulk Y_2O_2S phosphors, doped with Er^{3+} and co-doped with Yb^{3+} and Er^{3+}, were successfully prepared in high purity using the solid-state polysulfide flux method. The morphology and structure characterized using TEM showed that the as-prepared oxysulfide phosphors clearly exhibited a spherical morphology with the exception of a few irregular hexagonal facet pieces. A rather large particle size distribution ranging from 2 - 5 μm was also observed. The crystallite size was determined to be approximately 35 nm using the Scherer equation and it is concluded that the irregular morphology and large distribution of particle sizes observed from the TEM micrographs is attributed to the aggregation of crystallites during the calcination process which had agglomeration to form the larger spherical particles. The XRD diffraction pattern consisted primarily of the Y_2O_2S phase and no evidence of Y_2O_3 or fluxing agents was observed indicating that the sulfurization process of Y_2O_3 was complete. Also, the absence of Yb_2O_2S and Er_2O_2S diffraction peaks suggested that the Yb^{3+} and Er^{3+} ions are well dispersed throughout the Y_2O_2S lattice.

Regardless of the excitation wavelength used, the UC emission spectra obtained for all samples possessed the same spectral profile and was independent of the Yb^{3+} and Er^{3+} dopants as well as their respected concentrations. The green and red emissions occurring near 530 and 550 nm and 660 - 670 nm were consistent with the $(^2H_{11/2})^4S_{3/2} \rightarrow {}^4I_{15/2}$ and $^4F_{9/2} \rightarrow {}^4I_{15/2}$ transitions, respectively. The UC mechanisms excited at 808, 980, and 1560 nm were thoroughly discussed and investigated in detail. Monitoring the 547

and 670 nm emission peaks under both 808 and 980 nm excitation, the power dependent behavior on the UC emission intensities for singly doped Er^{3+} Y_2O_2S phosphors indicated that a two-photon excitation process was required for populating the $^4S_{3/2}$ and $^4F_{9/2}$ emitting states. Likewise, the Yb^{3+} and Er^{3+} co-doped phosphors excited at 980 nm also indicated a two-photon excitation process.

Y_2O_2S doped with 10% Er^{3+} showed the most intense UC emissions under 808 and 1560 nm excitation. Y_2O_2S co-doped with 15% Yb^{3+} and 3% Er^{3+} showed the most intense emissions under 980 nm excitation. Co-doping higher Er^{3+} concentrations in the 5% Yb^{3+} Y_2O_2S phosphors lead to a significant increase in the intensity of the red emission band accompanied by a decrease in the intensity of the green emission band. The observable changes in the intensity of the green and red emission bands were attributed to the non-radiative $^4F_{7/2} \rightarrow {}^4F_{9/2}$ and $^4I_{13/2} \rightarrow {}^4I_{15/2}$ transitions which became more predominant as the concentration of Er^{3+} reached nearly that of Yb^{3+}. Upon 1560 nm excitation, the intensity of the red emission band was significantly enhanced by co-doping Er^{3+} with Yb^{3+}. Two different ET mechanisms believed to be the most plausible were proposed, schematically shown, and addressed in detail. The effects of concentration quenching became apparent when either the concentration of erbium or ytterbium reached 20%, respectively.

References

[1] Wei, Y.; Lu, F.; Zhang, X.; Chen, D., *Journal of Alloys and Compounds*, 427, **2006** 333-340

[2] Liu, Z, Sun, X.; Xu, S.; Lian, J.; Li, X,; Xiu, Z.; Li, Q.; Huo, D.; Li, J., *J. Phys. Chem. C*, 112, **2008**, 2353-2358

[3] Vertone, F.; Boyer, J.; Speghini, A.; Bettinelli, M.; Capobianco, J., *J. App. Physics*, 96**, 2004**, 661-667

[4] Vertone, F.; Boyer, J.; Capobianco, J.; Speghini, A.; Bettinelli, M.*, Chem. Mater.*, 15**, 2003**, 2737-2743

[5] Glaspell, G.; Anderson, J.; Wilkins, J.R.; El-Shall, M.S., *J. Phys. Chem. C*, 112, **2008**, 11527-11531

[6] Silver, J.; Martinez-Rubio, M.; Ireland, T.; Fern, G.; Whitnall, R., *J. Phys. Chem. B*, 105, **2001**, 948-953

[7] Xiao, S.; Yang, X.; Liu, Z.; Yan, X.H., *J. App. Physics,* 96, **2004** 1360-1364

[8] XiXian, L.;WangHe, C., *Sci. Ser B-Chem*, 50, **2007**, 505-513

[9] Yi, Guang-Shun; Chow, Gan-Moog., *J. Mater. Chem.*, 15, **2005**, 4460-4464

[10] Yang, X.; Xiao, S.; Jing, J.W.; Yan, X.H., *J. Mater. Sci.*, Vol. 42, **2007**, 7042-7045

[11] Wang, Y.; Ohwaki, J., *J. App. Physics,* Vol. 74, **1993** 1272-1278

[12] Mahalingam, V.; Mangiarini, F.; Vetrone, F.; Venkatramu, V.; Bettinelli, M.; Speghini, A.; Capobianco, J., *J. Phys. Chem. C Letters*, 112, **2008**, 17745-17749

[13] Rakov, N.; Guimaraes, R.B.; Maciel, G.S.; *Appl. Phys. B*, 98, **2010**, 435-438

[14] Vertone, F.; Boyer, J.; Capobianco, J.; Speghini, A.; Bettinelli, M*., J. Phys. Chem. B*, 107**, 2003**, 1107-1112

[15] Prasad, P.N., *Nanophotonics*; John Wiley and Sons: New York, 2004

[16] Kuisheng, Y.; Yan, L.; Chaoyi, Y.; Liping, L.; Chanhua, Y.; Xiyan, Z., *J. Rare Earths*, 24, **2006**, 757-760

[17] Luo, Xi-xian; Cao, Wang-he, *Materials Letters*, 61, **2007**, 3696-3700

[18] Kawahara, Y.; Petrykin, V.; Ichihara, T.; Kijima, N.; Kakihana, M., *Chem. Mater.*, 18, **2006**, 6303-6307

[19] Bang, J.; Abboudi, M.; Abrams, B.; Holloway, P.H., *J. Luminescence*, 106, **2004**, 177-185

[20] Hang, T.; Liu, Q.; Mao, D.; Chang, C., *Materials Chemistry and Physics*, 107, **2008**, 142-147

[21] Kuang, J.; Liu, Y.; Yuan, D., *Electrochemical and Solid-State Letters*, 8, **2005**, H72-H74

[22] Lo, Chung-Lun.; Duh, Jeng-Gong.; Chiou, Bi-Shiou.; Peng, Chao-Chi.; Ozawa, L., *Materials Chemistry and Physics*, 71, **2001**, 179-189

[23] Kottaisamy, M.; Jagannathan, R.; Rao, R.P.; Avudaithai, M.; Srinivasan, L.K.; Sundaram, V., *J. Electrochem. Soc*., 142, **1995**, 3205-3209

[24] Georgobiani, A.N.; Bogatyreva, A.A.; Ishchenko, V.M.; Manashirov, O.Ya.; Gutan, V.B.; Semendyaev, S.V., *Inorganic Materials*, Vol. 43, **2007**, 1073-1079

[25] Vertone, F.; Boyer, J.; Speghini, A.; Bettinelli, M.; Capobianco, J., *J. Phys. Chem. B*, 107, **2003**, 10747-10752